Nuclear Physics B403 (1993) 633–667
North-Holland

NUCLEAR
PHYSICS B

Higher-order corrections to jet cross sections in hadron colliders

W.T. Giele [1]

Fermi National Accelerator Laboratory, P.O. Box 500, Batavia, IL 60510, USA

E.W.N. Glover [2]

Physics Department, University of Durham, Durham DH1 3LE, UK

David A. Kosower [3]

Theory Division, CERN, CH-1211 Geneva 23, Switzerland and Service de Physique Théorique, Centre d'Etudes de Saclay, F-91191 Gif-sur-Yvette cedex, France [4]

Received 17 December 1992
Accepted for publication 2 February 1993

We describe a general method of calculating the fully differential cross section for the production of jets at next-to-leading order in a hadron collider. This method is based on a "crossing" of next-to-leading order calculations with all partons in the final state. The method introduces universal crossing functions that allow a modular approach to next-to-leading order calculations for any process with initial state partons. These techniques are applied to the production of jets in association with a vector boson including all decay correlations of the final state observables.

1. Introduction

One of the most striking features of hadronic events is the appearance of "jets" of hadrons. By use of a suitable experimental jet algorithm, the hadronic data may be organized into final states containing a definite number of jets. This defines the topological structure of the event for a given jet algorithm. Different jet algorithms or jet defining cuts can lead to a different number of jets being observed in a given event. As a result, jet cross sections depend on the procedure

[1] SSC Fellow. E-mail: giele@fnth02.fnal.gov.
[2] E-mail: ewng@hep.dur.ac.uk.
[3] E-mail: kosower@amoco.saclay.cea.fr.
[4] Laboratory of the Direction des Sciences de la Matière of the Comissariat à l'Energie Atomique of France.

used to define an experimental jet. Nevertheless, at the experimental level, a jet is a perfectly well defined quantity since for a given jet algorithm each event contains a precisely determined number of jets.

From the theoretical point of view, the jet algorithm plays an important role in selecting high momentum transfer events in which the soft radiation is removed by a cut on the minimal transverse energy of the jet. At the same time, individual hadron behavior is averaged out by replacing all hadrons within a cone of a given size by a single jet axis and jet energy. Because the hadronic information is averaged out, we can relate the hadronic jet axis and energy observed in the experiment to a jet axis and energy constructed from a parton shower calculated within perturbative VQCD . The jet axis and energy obtained from the hadronic shower are thus modelled by the jet axis and energy obtained from the parton shower. This is a weak form of the parton–hadron duality theorem [1]. Of course, non-perturbative hadronization effects are not predicted by perturbative QCD. Similarly, the contributions from the underlying event (at hadron colliders) are not included. "Sensible" jet algorithms minimize these effects and allow a more direct comparison between theory and experiment.

More precise theoretical predictions of jet cross sections are potentially valuable since new physics is often evident in events containing a specific number of jets. The corresponding QCD background is then the exclusive jet cross section containing the same number of jets. For example, the signal to background ratio for the top quark in the lepton + jets channel is improved by demanding that more jets be observed [2].

The lowest order matrix elements for the two most prominent processes containing jets at hadron colliders,

$$p\bar{p} \to n_1 \text{ jets}, \tag{1.1}$$

$$p\bar{p} \to W^{\pm}Z + n_2 \text{ jets}, \tag{1.2}$$

have been computed for $n_1 \leqslant 5$ [3] and $n_2 \leqslant 4$ [4] by making use of helicity amplitudes [5], color decompositions [6–8] and recursion relations [9,10] to control the rapid increase in the number of Feynman diagrams as the number of partons involved grows. The jet cross section is then obtained by Monte Carlo integration of the phase space of the final state partons. This approach allows any experimental jet algorithm and acceptance to be applied, and one can study any distribution depending on the jet observables. It is important to note that at leading order, the jet is modelled by a single parton. The jet defining cuts are applied to this lone parton and the parton's direction and energy describe the jet's axis and energy *.

Comparisons of lowest order QCD predictions of jet distributions with the

* Including higher orders would give contributions where this parton has generated a "shower"; the jet clustering will nonetheless reconstruct closely the leading order estimate of the jet axis and energy (assuming an ideal detector), as a consequence of energy–momentum conservation.

data have proved reasonable, bearing in mind the fact that one is comparing a theoretical perturbative calculation with hadronic data. Generally, the shapes of infrared safe distributions are well predicted while the overall normalization is uncertain, due to a dependence on the unphysical renormalization and factorization scales μ_R and μ_F [11].

The addition of next-to-leading order effects produces three important improvements over a leading order calculation. First, the dependence on the unphysical scales μ_R and μ_F is reduced so that the normalization is more certain. Second, we begin to reconstruct the parton shower. This means that two partons may combine to form a single jet. As a result, jet cross sections become sensitive to the details of the jet-finding algorithm, particularly the way in which the hadrons are combined to form the jet axis and energy, and to the size of a jet cone. This sensitivity is also seen in experimental results. Third, the calculation becomes more sensitive to detector limitations, because radiation outside the detector is simulated. This can change leading order results considerably for quantities such as the missing transverse energy in events containing a W-boson.

From a more theoretical point of view, the presence of infrared logarithms in a generic perturbative QCD prediction implies that the expansion of physical quantities is not strictly a series in the coupling constant α_s, but is rather a series in $\alpha_s \ln^2 y_{IR}$ and $\alpha_s \ln y_{IR}$ (as well as α_s alone), where y_{IR} is an experimental resolution (for example, the minimum jet invariant mass in $e^- e^+$ collisions). Thus even in the perturbative regime, the leading order result—where the size of these logarithms is uncalculated—suffers from potentially large corrections which might spoil the applicability of perturbative QCD. In a next-to-leading order calculation, these logarithms are calculated explicitly, and thus one regains confidence in the applicability of the perturbative expansion. From this purist's point of view, a next-to-leading order calculation is necessary in order to understand whether a leading order result is trustworthy.

At next-to-leading order, the n-jet cross section receives contributions from virtual corrections to n-parton, and from real corrections in the form of $(n+1)$-parton final states. Both contributions are divergent. The matrix elements for the virtual diagrams are infrared divergent, while the real $(n+1)$-parton matrix elements are well defined. However, when the $(n+1)$-parton matrix elements are integrated over the allowed regions of phase space an infrared-divergent cross section is obtained. This comes about because the jet algorithm allows one of the partons to be soft, or for two partons within a jet cone to be collinear.

In order to cancel these divergences explicitly, it is convenient to divide the $(n+1)$-parton phase space into regions where $(n+1)$-partons are "resolved" and regions where only n-partons are "resolved" [12–14]*. For example, if the

* Note that this approach is different from that described in refs. [15–17] and we refer the reader to the introduction of ref. [16] for a lucid explanation of the difference between the two methods.

invariant mass of two partons, s_{ij}, is smaller than some theoretical parton resolution parameter $s_{\min}$ only one parton is resolved, while if $s_{ij} > s_{\min}$ both partons are resolved. All of the divergences from the $(n+1)$-parton final state separate and are associated with the regions where only n-partons are resolved. These divergences can be cancelled directly against the virtual corrections to the n-parton cross section. With such a physical picture* it is straightforward to extend this method to deal with any number of partons in the final state. Indeed, using a color decomposition of the amplitude, one can write down a simple soft factorization [18] for the sub-amplitudes, which in turn allows the construction of a universal set of functions summarizing the soft and collinear behavior of the matrix element of any colored particles, both before and after the cancellation of infrared divergences described above. Recently, we have described how this scheme may be applied to multijet cross sections in e^-e^+ annihilation [14]. This case is rather special since there can be no QCD radiation in the initial state and all divergences therefore reside in the final state. In the paper, we wish to extend this method to processes which involve partons in the initial state.

In section 2, we show how to set up the next-to-leading order calculation of the matrix elements for $e^-e^+ \to n$ partons and how they may be "crossed" to give the cross section for $p\bar{p} \to V + (n-2)$ partons where $V = W^{\pm}, \gamma^*, Z$. In order to do this it is convenient to introduce (in addition to the universal soft and collinear functions mentioned above) a set of universal crossing functions which multiply the lowest order cross section. These crossing functions are essentially convolutions of the input structure functions with the Altarelli–Parisi splitting functions. Section 3 deals with the derivation of the crossing functions which enable us to cross final state partons to the initial state. In section 4, we construct explicit Monte Carlo programs for

$$p\bar{p} \to V + 0,1 \text{ jets} \to \ell\bar{\ell}' + 0,1 \text{ jets}, \tag{1.3}$$

at next-to-leading order. The jet algorithm may then be applied directly to the n- and $(n+1)$-parton final states. All dependence on the unphysical parton resolution parameter $s_{\min}$ cancels numerically . The cross section is fully differential in all jet and lepton observables and therefore differs from calculations of the W transverse momentum distribution at $O(\alpha_s^2)$ [19,20] or of the single jet inclusive transverse momentum distribution at $O(\alpha_s^3)$ [13,21]. Equivalent techniques have been applied to $p\bar{p} \to W^{\pm} + 0$ jets [22] and $p\bar{p} \to 2$ jets [23] at next-to-leading order. Finally, we summarize our results in section 5.

* Although the parton resolution parameter is unphysical because partons are not directly observable, this concept parallels the way in which a calorimeter resolves physical particles.

2. Calculational organization

In this section we give a general overview of the manner in which the calculation is set up, without going into details, which we shall present in subsequent sections. The organization minimizes the computational effort while retaining the standard $\overline{\text{MS}}$ prescription [24]. For example, the cumbersome d-dimensional squaring of the matrix elements is avoided. Furthermore, the introduction of universal crossing functions will allow us to obtain the initial state parton cross sections from the all-outgoing cross section. These techniques depend crucially on the universality of the QCD soft and collinear radiation patterns.

An efficient way of organizing next-to-leading order calculations for all-outgoing parton processes was given in ref. [14]. The basis of this method is the use of ordered amplitudes associated with each color structure rather than the full matrix element. For example, let us consider the decay of a vector boson into a quark–antiquark pair with n accompanying gluons. The full squared amplitude is obtained by summing the squared ordered amplitudes over all permutations of the gluons [6–8],

$$|\mathcal{M}_V(V \to q\bar{q} + n\,g)|^2 \sim \sum_{\text{Perm.}} |A(q; g_1, \ldots, g_n; \bar{q})|^2 \,. \tag{2.1}$$

For simplicity, we keep only the terms at leading order in the number of colors. See section 4 for a full discussion of the subleading terms. Of crucial importance is the fact that the ordered amplitudes exhibit QED-like factorization [25] in the soft and collinear limits [18]. This forms the basis of our method and allows the integration over the singular (or unresolved) parts of phase space without calculating the hard matrix element explicitly,

$$\begin{aligned} &\int \mathrm{d}P_{\text{soft/collinear}} \, |A(q'; g'_1, \ldots, g'_{n+1}; \bar{q}')|^2 \\ &\quad \to R(q; g_1, \ldots, g_n; \bar{q}|s_{\min}) \, |A(q; g_1, \ldots, g_n; \bar{q})|^2 \,, \end{aligned} \tag{2.2}$$

where the soft and collinear regions of phase space are defined by the invariant mass cut $s_{\min}$. At this point everything is done in an arbitrary number of dimensions [26,27]. However, we never have to calculate the hard amplitude squared explicitly since this result is obtained without any detailed knowledge of the hard process. The next step is to calculate the virtual corrections to the squared matrix elements, which have the generic form,

$$\begin{aligned} |\mathcal{M}_V(V \to q\bar{q} + n\,g)|_V^2 \;=\; &\sum_{\text{Perm.}} V(q; g_1, \ldots, g_n; \bar{q}) \; |A(q; g_1, \ldots, g_n; \bar{q})|^2 \\ &+ \mathcal{F}(q; g_1, \ldots, g_n; \bar{q}), \end{aligned} \tag{2.3}$$

where $V(q; g_1, \ldots, g_n; \bar{q})$ is the singular part proportional to the tree level ordered amplitude and $\mathcal{F}(q; g_1, \ldots, g_n; \bar{q})$ is the remaining finite contribution.

This can be immediately combined with the unresolved phase space contribution eq. (2.2) to give the finite next-to-leading order squared matrix elements,

$$|\mathcal{M}_V(V \to q\bar{q} + n\,g)|_F^2 \sim \sum_{\text{Perm.}} \Big(\quad [1 + \mathcal{K}]\,|A(q; g_1, \ldots, g_n; \bar{q})|^2 + \mathcal{F}(q; g_1, \ldots, g_n; \bar{q}) \Big). \tag{2.4}$$

Note that due to the Kinoshita–Lee–Nauenberg [28,29] theorem the combination of the phase space factor and the virtual factor, $\mathcal{K} = R + V$, is finite. As a direct consequence we can now perform the squaring and summation over the polarizations in four dimensions using the standard techniques developed for evaluating complicated tree level amplitudes (helicities [5] and recurrence relations [9]). While V can be calculated in a process independent manner [14], the finite remainder of the virtual correction $\mathcal{F}$ needs to be calculated on a process-by-process basis. The general structure is process independent, and it is in this sense that the $\mathcal{K}$ factor is universal.

In order to generalize the framework above, used in e^-e^+ collisions, to hadronic collisions, we must include initial state partons in the calculation. One useful property of lowest order matrix elements is that of "crossing". In other words, the matrix elements for $V \to q\bar{q} + n\,g$ are related to those for the crossed processes

$$\begin{aligned} q\bar{q} &\to V + n\,g, \\ qg &\to V + q + (n-1)\,g, \\ \bar{q}g &\to V + q + (n-1)\,g, \\ gg &\to V + q\bar{q} + (n-2)\,g, \end{aligned} \tag{2.5}$$

by reversal of the momentum and helicity of the crossed particles. The fully differential cross section at leading order in the collision of hadrons H_1 and H_2,

$$H_1 + H_2 \to V + n\,\text{partons}, \tag{2.6}$$

is

$$\mathrm{d}\sigma_{H_1H_2} = \sum_{ab} f_a^{H_1}(x_1)\, f_b^{H_2}(x_2)\, \mathrm{d}\sigma_{ab}^{\mathrm{LO}}(x_1, x_2)\, \mathrm{d}x_1\, \mathrm{d}x_2. \tag{2.7}$$

Here $f_a^H(x)$ is the probability density of finding parton a in hadron H with momentum fraction x and,

$$\mathrm{d}\sigma_{ab}^{\mathrm{LO}}(x_1, x_2) = \frac{\Phi_{ab}}{2\,s_{ab}}\,|\mathcal{M}_{ab}|^2\ \mathrm{d}P(ab \to V + n\,\text{partons}), \tag{2.8}$$

where Φ_{ab} is the appropriate spin and color averaging factor and $\mathrm{d}P$ the $V + n$-parton phase space where all parton pairs satisfy $s_{ij} > s_{\min}$. The matrix elements for $ab \to V + n$ partons are denoted $|\mathcal{M}_{ab}|^2$ and are related by crossing to $|\mathcal{M}_V|^2$, eq. (2.1).

We have already discussed how the next-to-leading order matrix elements for $e^-e^+ \to n$ partons can be written in an explicitly finite way using the parton resolution parameter $s_{\min}$. We now wish to extend this to processes involving partons in the initial state while maintaining the crossing properties of lowest order. In order to achieve this, the next-to-leading order hadronic cross section must be defined by

$$d\sigma_{H_1H_2} = \sum_{ab} \mathcal{F}_a^{H_1}(x_1)\mathcal{F}_b^{H_2}(x_2)\, d\sigma_{ab}^{\mathrm{NLO}}(x_1,x_2)\, dx_1\, dx_2, \tag{2.9}$$

where $\mathcal{F}_a^H$ is the "effective" next-to-leading order structure function and $d\sigma_{ab}^{\mathrm{NLO}}$ the "crossed" analog of the finite next-to-leading order partonic cross section. This cross section can be expanded as a series in the coupling constant,

$$d\sigma_{ab}^{\mathrm{NLO}} = d\sigma_{ab}^{\mathrm{LO}} + \alpha_s\, d\,\delta\sigma_{ab}^{\mathrm{NLO}} + O(\alpha_s^2), \tag{2.10}$$

where we have extracted the coupling constant from the finite crossed matrix elements. Note that α_s is evaluated at the renormalization scale μ_R. Similarly, after mass factorization, the effective structure function $\mathcal{F}_a^H$ may be written as

$$\mathcal{F}_a^H(x) = f_a^H(x,\mu_F) + \alpha_s\, C_a^H(x,\mu_F) + O(\alpha_s^2), \tag{2.11}$$

where μ_F is the factorization scale. Both $f_a^H(x,\mu_F)$ and the crossing function $C_a^H(x,\mu_F)$ are finite. Once again α_s is evaluated at the renormalization scale. In principle one could evaluate α_s at the mass factorization scale, however, provided $\alpha_s \log(\mu_R^2/\mu_F^2) \ll 1$, the difference is of $O(\alpha_s^2)$ and can be ignored. For a detailed derivation of the structure of the crossing function C_a^H we refer the reader to section 3.

Inserting these definitions back into eq. (2.9) and expanding up to $O(\alpha_s)$ we find

$$\begin{aligned} d\sigma_{H_1H_2} = \sum_{ab} \Big[& f_a^{H_1}(x_1) f_b^{H_2}(x_2) \left\{ d\sigma_{ab}^{\mathrm{LO}}(x_1,x_2) + \alpha_s\, d\,\delta\sigma_{ab}^{\mathrm{NLO}}(x_1,x_2) \right\} \\ & + \alpha_s \left\{ C_a^{H_1}(x_1) f_b^{H_2}(x_2) + f_a^{H_1}(x_1) C_b^{H_2}(x_2) \right\} d\sigma_{ab}^{\mathrm{LO}}(x_1,x_2) \\ & + O(\alpha_s^2) \Big]\, dx_1\, dx_2. \end{aligned} \tag{2.12}$$

For simplicity, we have suppressed the dependence on the renormalization scale in the coupling constant and the factorization scale in the structure and crossing functions.

The crossing function receives two contributions which both stem from the fact that we consider two partons to be unresolved when their invariant mass is smaller than the parton resolution parameter $s_{\min}$. Firstly, we cannot distinguish between a single initial state parton and a parton which emits collinear radiation such that the invariant mass of the collinear pair is smaller than $s_{\min}$. This implies that part of the initial state collinear radiation is removed from the

hard scattering and absorbed into the effective structure function. Clearly, this contribution depends on $s_{\min}$ and therefore so do the crossing functions (and also $\mathcal{F}_a^H$). This term is a convolution of f_a^H with the Altarelli–Parisi splitting function, $P_{a\to c}(z)$ [30].

The second contribution arises from crossing a pair of collinear partons with an invariant mass smaller than $s_{\min}$ from the final state to the initial state. In principle we should remove this contribution from $\mathrm{d}\,\delta\sigma_{ab}^{\mathrm{NLO}}$; however, in order to preserve the structure of eq. (2.9), we subtract this contribution from the parton density function. This is possible because we cannot distinguish the two-parton incoming state with invariant mass smaller than $s_{\min}$ from a single incoming parton.

Both of these contributions are divergent and schematically

$$C_a^H(x) \sim \sum_c \left[\int_x^1 \frac{\mathrm{d}z}{z} f_c^H(x/z)\, P_{c\to a}(z) - f_a^H(x) \int_0^1 \mathrm{d}z\, P_{a\to c}(z) \right] \frac{s_{\min}^{-\epsilon}}{\epsilon}. \tag{2.13}$$

A more precise formulation of the crossing function is given in the next section including all d-dimensional factors. After mass factorization the crossing function is rendered finite,

$$C_a^{H,\mathrm{scheme}}(x,\mu_{\mathrm{F}}) = \left(\frac{N}{2\pi}\right) \left[A_a^H(x) \log\left(s_{\min}/\mu_{\mathrm{F}}^2\right) + B_a^{H,\mathrm{scheme}}(x) \right]. \tag{2.14}$$

Although A_a^H is scheme independent, B_a^H does depend on the mass factorization scheme and therefore so does C_a^H. Explicit forms for these functions in the $\overline{\mathrm{MS}}$ scheme are given in the next section.

The overall cross section cannot depend on the unphysical parameter $s_{\min}$. When the contribution from $H_1 + H_2 \to V + (n+1)$ partons where all partons are resolved is included, the $s_{\min}$ in the logarithm is replaced by an energy scale defined by the experimental cuts. In a numerical computation, one would also force the factorization scale to be determined by the experimental cuts; the argument of the logarithm would then be of O(1) and the contribution from A_a^H would be small. If this were not true, the logarithm would be large so that $\alpha_{\mathrm{s}} A_a^H(x) \log\left(E_{\mathrm{exp}}^2/\mu_{\mathrm{F}}^2\right) \simeq f_a^H(x)$, perturbation theory would break down and a resummation of the leading logarithms would be necessary.

3. Derivation of the crossing functions

In this section we derive explicit formulae for the crossing functions $C_a^H(x,\mu_{\mathrm{F}})$ as defined in eqs. (2.9)–(2.12). First, we derive the initial state collinear phase space behavior in a parametrization suitable for our parton resolution parameter. We then reformulate the standard collinear matrix element factorization in the ordered amplitude language. Combining these results enables us to derive the

universal crossing functions which after mass factorization yield finite crossing functions.

3.1. THE INITIAL STATE COLLINEAR BEHAVIOR OF PHASE SPACE

First consider the production of a heavy object, Q, by the collision of two massless particles with momenta p_a and p_h. The d-dimensional phase space measure, including the flux factor, is given by

$$\frac{1}{2s_{ah}}\mathrm{d}P^d(a+h\to Q)=\frac{2\pi}{2s_{ah}}\delta(s_{ah}-Q^2), \tag{3.1}$$

where $s_{ah}=(p_a+p_h)^2$. This extends straightforwardly to the production of any number of particles (massless or otherwise) with momenta $p_1,\ldots,p_n$ by use of the relation

$$\mathrm{d}P^d(a+h\to 1+\ldots+n)=\mathrm{d}P^d(a+h\to Q)\frac{\mathrm{d}Q^2}{2\pi}\mathrm{d}P^d(Q\to 1+\ldots+n). \tag{3.2}$$

Next consider the phase space for the production of a massless particle with momentum p_u in association with Q from the collision of two massless particles with momenta p_a and p_p,

$$\begin{aligned}\frac{1}{2s_{ap}}\mathrm{d}P^d(a+p\to u+Q) &= (2\pi)^{2-d}\frac{\underline{\mathrm{d}}|s_{au}|\,\underline{\mathrm{d}}|s_{pu}|}{s_{ap}^2}\left(\frac{|s_{au}||s_{pu}|}{s_{ap}}\right)^{-(2-d/2)}\\ &\quad\times\tfrac{1}{8}\mathrm{d}\Omega_{d-3}\,\delta(s_{ap}-|s_{au}|-|s_{pu}|-Q^2),\end{aligned} \tag{3.3}$$

where we integrate over the invariant mass of Q and the polar angle with respect to p_p by using $|s_{au}|$ and $|s_{pu}|$, as well as integrating over the $(d-3)$ azimuthal angles relative to the direction of p_p.

The region where momentum p_u is collinear with momentum p_p is defined by

$$|s_{pu}|<s_{\min}. \tag{3.4}$$

In this region we introduce the hard momentum p_h, which is the amount of the parent momentum p_p remaining after the emission of the unobserved collinear momentum p_u such that

$$\begin{aligned}p_h &= zp_p, & s_{ah} &= zs_{ap},\\ p_u &= (1-z)p_p, & |s_{au}| &= (1-z)s_{ap}.\end{aligned} \tag{3.5}$$

In this limit the phase space factorizes,

$$\frac{1}{2s_{ap}}\mathrm{d}P^d(a+p\to u+Q)\to\mathrm{d}P^d_{\mathrm{col}}(p\to u+h)\times\frac{1}{2s_{ah}}\mathrm{d}P^d(a+h\to Q), \tag{3.6}$$

where, taking $d = 4 - 2\epsilon$, we find

$$\mathrm{d}P_{\mathrm{col}}^{4-2\epsilon}(p \to u + h) = \frac{(4\pi)^{\epsilon}}{16\pi^2\Gamma(1-\epsilon)} z\,\mathrm{d}z\,\mathrm{d}|s_{pu}|\,[(1-z)|s_{pu}|]^{-\epsilon}. \quad (3.7)$$

The square bracket contains the necessary factors to regulate the poles in the matrix elements in $(1 - z)$ and s_{pu}.

Combining these results we find that in the collinear limit, the full phase space measure of interest factorizes as follows:

$$\mathrm{d}P^d(a + p \to u + 2 + \ldots + n) = \mathrm{d}P_{\mathrm{col}}^d(p \to u + h) \times \frac{1}{s_{ah}}\,\mathrm{d}P^d(a + h \to 2 + \ldots + n). \quad (3.8)$$

3.2. BEHAVIOR OF MATRIX ELEMENTS

The matrix elements also undergo a collinear factorization when one of the final state partons is collinear with one of the initial state partons. Take the case where an initial state parton p splits into partons u and h (which participates in the hard scattering) as in eq. (3.5); then, for each ordered amplitude,

$$\left|A(\ldots, p, u, n, \ldots)\right|^2 \to \hat{c}_{\mathrm{F}}^{p\to uh}\left|A(\ldots, h, n, \ldots)\right|^2, \quad (3.9)$$

where

$$\hat{c}_{\mathrm{F}}^{p\to uh} = \tfrac{1}{2}g^2 N \frac{1}{|s_{pu}|}\frac{\hat{P}_{hu\to p}(z)}{z}. \quad (3.10)$$

Note that the quantum numbers of the unobserved parton u are determined by the quantum numbers of the parent parton p and the hard process parton h.

This is very similar to the factorization that occurs when two final state particles are collinear. In this case, when parton a (which participates in the hard scattering) splits into a final state collinear parton pair 1 and 2,

$$\left|A(\ldots, 1, 2, \ldots)\right|^2 \to \hat{c}_{\mathrm{F}}^{12\to a}\left|A(\ldots, a, \ldots)\right|^2, \quad (3.11)$$

where

$$\hat{c}_{\mathrm{F}}^{12\to a} = \tfrac{1}{2}g^2 N \frac{1}{s_{12}}\hat{P}_{12-a}(z), \quad (3.12)$$

$$p_1 = zp_a, \qquad p_2 = (1-z)p_a. \quad (3.13)$$

The different averaging factors for initial and final state quarks and gluons have been taken into account; however, we do not sum here over different flavors of quarks participating in the hard process.

As before, the splitting functions may be either in the conventional scheme (all particles in d dimensions) [30] or in the 't Hooft–Veltman scheme (only

unobserved particles in d dimensions) [26]. In the conventional scheme, the splitting functions are given by

$$\begin{aligned}
\widehat{P}_{gg\to g}(z) &= P_{gg\to g}(z) = 4\left(\frac{z}{1-z} + \frac{1-z}{z} + z(1-z)\right), \\
\widehat{P}_{qg\to q}(z) &= \left(1 - \frac{1}{N^2}\right) P_{qg\to q}(z) = 2\left(1 - \frac{1}{N^2}\right)\left(\frac{1 + z^2 - \epsilon(1-z)^2}{1-z}\right), \\
\widehat{P}_{q\bar{q}\to g}(z) &= \frac{1}{N} P_{q\bar{q}\to g}(z) = \frac{2}{N}\left(\frac{z^2 + (1-z)^2 - \epsilon}{1-\epsilon}\right).
\end{aligned} \tag{3.14}$$

For the splitting functions in the 't Hooft–Veltman scheme, see ref. [26].

One difference from pure final state singularities is that the initial state parton is always hard—there is always a minimum value for z imposed by demanding that a hard scattering takes place. On the other hand, the upper bound on z is still determined by the requirement that parton u is collinear but not soft. In other words, $s_{un} > s_{\min}$, where n is the neighboring hard parton in the ordered amplitude [see eq. (3.9)].

For the $g \to gg$ process, there will be contributions from two ordered amplitudes,

$$\left|A(\ldots, m, p, u, n, \ldots)\right|^2 + \left|A(\ldots, m, u, p, n, \ldots)\right|^2 \to \left|A(\ldots, m, h, n, \ldots)\right|^2, \tag{3.15}$$

where the order of the other hard partons in the ordered amplitude is preserved. The upper limit on z will be different in each case since the requirement that gluon u be unobserved depends on the adjacent momenta. Note that in the final state case, each ordering counts equally, however, the Bose symmetry factor takes this into account. For processes involving collinear quarks (antiquarks), only one ordering will contribute. Note that only ordered amplitudes where p and u are adjacent contribute in the collinear limit. If they are not adjacent as in eq. (3.15) the collinear limit gives a contribution of the order of the parton resolution cut $s_{\min}$, which is therefore negligible. This property is very useful since it avoids overlapping divergences for a given ordered amplitude and this makes partial fractioning to isolate the divergences unnecessary.

3.3. BEHAVIOR OF THE CROSS SECTION

In this subsection we derive exact expressions for the crossing functions $C_a^H(x)$ or, equivalently, the effective structure function $\mathcal{F}_a^H(x)$ as defined in eqs. (2.9)–(2.12). We will consider the generic process of scattering of partons a and h to form an arbitrary final state with an invariant mass $\sqrt{Q^2}$ (e.g. partons only, vector boson plus partons, etc.). The leading order cross section for the production of a vector boson plus partons is given in eq. (2.7). Cross sections for other final

states are given by similar formulae. The next-to-leading order cross section is defined in eq. (2.9), or in its expanded form in eq. (2.12).

The first step in the derivation of the crossing function is to consider the initial state collinear radiation contribution to the next-to-leading order cross section. Consider the splitting of a parent parton p to a (unobserved) collinear parton u, and a parton h participating in the hard scattering: $p \to uh$, where the invariant mass $|s_{pu}| < s_{\min}$ so that this configuration is indistinguishable from the leading order configuration where parton h comes directly from the hadron. This contributes to the next-to-leading order cross section and using eqs. (3.7) and (3.9) we find

$$\begin{aligned} \mathrm{d}\sigma_{\text{initial}} = & \sum_{ahp} f_a^{H_1}(x_1) \left\{ f_p^{H_2}(y) \hat{c}_{\mathrm{F}}^{p\to uh} \, \mathrm{d}P_{\text{col}}^{d}(p \to u + h)\, \delta(x_2 - zy) \mathrm{d}y \right\} \\ & \times \mathrm{d}\sigma_{ah}^{\text{LO}}(x_1, x_2)\, \mathrm{d}x_1\, \mathrm{d}x_2, \end{aligned} \tag{3.16}$$

where, by definition, the momentum fraction x_2 carried by parton h is given by the momentum fraction y of the original parton p multiplied by the energy fraction remaining after radiating the unobserved parton u. There is an implicit integration over z contained in the collinear phase space factor, see eq. (3.7). Comparing eq. (3.16) with eq. (2.12) gives the contribution of the initial state radiation to the crossing function,

$$\alpha_{\mathrm{s}} C_{h,\,\text{initial}}^{H_2}(x_2) = \sum_{p} f_p^{H_2}(y) \hat{c}_{\mathrm{F}}^{p\to uh} \, \mathrm{d}P_{\text{col}}^{d}(p \to u + h)\, \delta(x_2 - zy)\, \mathrm{d}y. \tag{3.17}$$

Using eq. (3.10) and the collinear phase space factor of eq. (3.7) gives

$$\begin{aligned} C_{h,\,\text{initial}}^{H_2}(x_2) &= -\left(\frac{N}{2\pi}\right) \frac{1}{\Gamma(1-\epsilon)} \left(\frac{4\pi\mu^2}{s_{\min}}\right)^{\epsilon} \frac{1}{\epsilon} \\ &\quad \times \sum_{p} \frac{1}{4} \int_{x_2}^{1-z_2} \frac{\mathrm{d}z}{z} (1-z)^{-\epsilon} \hat{P}_{hu\to p}(z) f_p^{H_2}(x_2/z) \\ &= -\left(\frac{N}{2\pi}\right) \frac{1}{\Gamma(1-\epsilon)} \left(\frac{4\pi\mu^2}{s_{\min}}\right)^{\epsilon} \frac{1}{\epsilon} \\ &\quad \times \sum_{p} \int_{x_2}^{1} \frac{\mathrm{d}z}{z} f_p^{H}(x_2/z)\, J_{p\to h}(z, z_2)\,, \end{aligned} \tag{3.18}$$

where we have integrated y over the delta function and s_{pu} using the constraint $|s_{pu}| < s_{\min}$. Here μ is an arbitrary scale introduced to keep the strong coupling constant $\alpha_{\mathrm{s}} = g^2 \mu^{-2\epsilon}/4\pi$ dimensionless in d dimensions. The upper boundary on the z integral is determined by the constraint that the unobserved parton u is not soft with respect to its neighboring parton n. In other words, $|s_{un}| = (1-z)|s_{hn}| > s_{\min}$. Explicitly this gives

$$z < 1 - s_{\min}/|s_{hn}| = 1 - z_2. \tag{3.19}$$

Note that s_{hn} is only defined because of the use of the ordered amplitudes and is different for each ordering.

Looking at the definition of the splitting functions, eq. (3.14), we see that $J_{q\to g}$ and $J_{g\to q}$ do not depend on the upper boundary on z [up to negligible corrections of $O(s_{\min})$]. This is due to the absence of a singularity in the limit that the quark or antiquark becomes soft. In contrast, the $J_{g\to g}$ and $J_{q\to q}$ functions do contain a soft singularity, arising from the limit where the gluon becomes soft, and therefore do depend on z_2. In order to write these contributions to the crossing functions in the second form in eq. (3.18), we use the $(\,)_+$ prescription defined by

$$(F(z))_+ = \lim_{\beta\to 0}\left(\theta(1-z-\beta)F(z) - \delta(1-z-\beta)\int_0^{1-\beta} F(y)\,dy\right), \tag{3.20}$$

such that

$$\int_x^{1-z_2} dz\,\frac{g(z)}{(1-z)^{1+\epsilon}} = \int_x^1 dz\,\frac{g(z)}{[(1-z)^{1+\epsilon}]_+} + \left(\frac{z_2^{-\epsilon}-1}{\epsilon}\right) g(1), \tag{3.21}$$

$$\int_x^1 dz\,\frac{g(z)}{[(1-z)^{1+\epsilon}]_+} = \int_x^1 dz\,\frac{g(z)}{(1-z)_+} - \epsilon\int_x^1 dz\,g(z)\left(\frac{\log(1-z)}{1-z}\right)_+ + O(\epsilon^2), \tag{3.22}$$

$$\int_x^1 dz\,\frac{g(z)}{(1-z)_+} = \int_x^1 dz\,\frac{g(z)-g(1)}{1-z} + g(1)\log(1-x), \tag{3.23}$$

$$\int_x^1 dz\,g(z)\left(\frac{\log(1-z)}{1-z}\right)_+ = \int_x^1 dz\,\frac{g(z)-g(1)}{1-z}\log(1-z) + \tfrac{1}{2}g(1)\log^2(1-x), \tag{3.24}$$

provided that $g(z)$ is a function well behaved at $z = 1$.

The functions $J_{p\to h}$ are thus given by

$$J_{g\to g}(z,z_2) = \left(\frac{z_2^{-\epsilon}-1}{\epsilon}\right)\delta(1-z) + \frac{z}{[(1-z)^{1+\epsilon}]_+} + \frac{(1-z)^{1-\epsilon}}{z} + z(1-z)^{1-\epsilon} + O(s_{\min}),$$

$$J_{q\to q}(z,z_2) = \left(1-\frac{1}{N^2}\right)\left\{\left(\frac{z_2^{-\epsilon}-1}{\epsilon}\right)\delta(1-z) + \frac{1}{2}\left(\frac{1+z^2}{[(1-z)^{1+\epsilon}]_+} - \epsilon(1-z)^{1-\epsilon}\right)\right\} + O(s_{\min}),$$

$$J_{q\to g}(z,z_2) = \tfrac{1}{4}\widehat{P}_{gq\to q}(z)(1-z)^{-\epsilon} + \mathrm{O}(s_{\min}),$$
$$J_{g\to q}(z,z_2) = \tfrac{1}{4}\widehat{P}_{q\bar{q}\to g}(z)(1-z)^{-\epsilon} + \mathrm{O}(s_{\min}). \tag{3.25}$$

The next step is to correct for the fact that we have crossed a final state collinear cluster to the initial state. As explained in section 2 this is done by subtracting the collinear factor resulting from the splitting $h \to up$ integrated over the final state collinear phase space (see ref. [14] for a detailed derivation). The contribution to the next-to leading order cross section is given by

$$\mathrm{d}\sigma_{\text{final}} = \sum_{ahp} f_a^{H_1}(x_1)\left\{f_h^{H_2}(x_2)\widehat{c}_{\mathrm{F}}^{pu\to h}\,\mathrm{d}P^d_{\text{col,final}}(h\to u+p)\right\}$$
$$\times\, \mathrm{d}\sigma^{\mathrm{LO}}_{ah}(x_1,x_2)\,\mathrm{d}x_1\,\mathrm{d}x_2, \tag{3.26}$$

giving

$$\alpha_{\mathrm{s}} C^{H_2}_{h,\text{final}}(x_2) = f_h^{H_2}(x_2)\sum_p \widehat{c}_{\mathrm{F}}^{pu\to h}\,\mathrm{d}P^d_{\text{col,final}}(h\to u+p)$$
$$= -\left(\frac{\alpha_{\mathrm{s}}N}{2\pi}\right)\frac{1}{\Gamma(1-\epsilon)}\left(\frac{4\pi\mu^2}{s_{\min}}\right)^{\epsilon} f_h^{H_2}(x_2)\frac{1}{\epsilon}\sum_p I_{pu\to h}(z_1,z_2). \tag{3.27}$$

Note that the parton density function is associated with parton h rather than with parton p. The integration boundaries of the z integral are again defined through the requirement that the hard partons are resolved. For each ordered amplitude z_1 and z_2 are given by demanding that the invariant mass of parton u with both its neighbors in the particular ordering is larger than the parton resolution cut $s_{\min}$ so that u is not soft. In the conventional scheme, the final state integrals over the splitting functions, $I_{pu\to h}$, are given by

$$I_{pu\to h}(z_1,z_2) = \frac{1}{4}\int_{z_1}^{1-z_2}\mathrm{d}z\,[z(1-z)]^{-\epsilon}\,\widehat{P}_{pu\to h}(z), \tag{3.28}$$

where

$$I_{gg\to g}(z_1,z_2) = \left(\frac{z_1^{-\epsilon}+z_2^{-\epsilon}-2}{\epsilon}\right) - \frac{11}{6} + \left(\frac{\pi^2}{3}-\frac{67}{18}\right)\epsilon + \mathrm{O}(\epsilon^2),$$
$$I_{qg\to q}(z_1,z_2) = \left(1-\frac{1}{N^2}\right)\left[\left(\frac{z_2^{-\epsilon}-1}{\epsilon}\right) - \frac{3}{4} + \left(\frac{\pi^2}{6}-\frac{7}{4}\right)\epsilon\right] + \mathrm{O}(\epsilon^2),$$
$$I_{qq\to g}(z_1,z_2) = \frac{1}{N}\left(\frac{1}{3}+\frac{5}{9}\epsilon\right) + \mathrm{O}(\epsilon^2). \tag{3.29}$$

We can now define the crossing function as a convolution integral involving the parton density function and a crossing kernel $X_{p\to h}(z)$ which is obtained by subtracting the final state contribution given by eq. (3.29) from the initial state

contributions of eq. (3.25),

$$\begin{aligned} C_h^H(x) &= C_{h,\,\text{initial}}^H(x) - C_{h,\,\text{final}}^H(x) \\ &= \sum_p \int_x^1 \frac{\mathrm{d}z}{z} f_p^H(x/z)\, X_{p\to h}(z), \end{aligned} \tag{3.30}$$

where the crossing kernel for specific processes is given by

$$\begin{aligned} X_{g\to g}(z) &= -\left(\frac{N}{2\pi}\right)\frac{1}{\Gamma(1-\epsilon)}\left(\frac{4\pi\mu^2}{s_{\min}}\right)^{\epsilon}\frac{1}{\epsilon} \\ &\quad\times\Big[J_{g\to g}(z,z_1) + J_{g\to g}(z,z_2) \\ &\quad -\Big(I_{gg\to g}(z_1,z_2) + \frac{n_f}{N} I_{q\bar q\to g}(0,0)\Big)\delta(1-z)\Big] \\ &= -\left(\frac{N}{2\pi}\right)\frac{1}{\Gamma(1-\epsilon)}\left(\frac{4\pi\mu^2}{s_{\min}}\right)^{\epsilon} \\ &\quad\times\frac{1}{\epsilon}\Big[2\left(\frac{z}{[(1-z)^{1+\epsilon}]_+} + \frac{(1-z)^{1-\epsilon}}{z} + z(1-z)^{1-\epsilon}\right) \\ &\quad + \left(\left(\frac{11N-2n_f}{6N}\right) - \epsilon\left(\frac{\pi^2}{3} - \frac{67}{18} + \frac{5n_f}{9N}\right)\right)\delta(1-z)\Big], \\ X_{q\to q}(z) &= -\left(\frac{N}{2\pi}\right)\frac{1}{\Gamma(1-\epsilon)}\left(\frac{4\pi\mu^2}{s_{\min}}\right)^{\epsilon} \\ &\quad\times\frac{1}{\epsilon}\Big(J_{q\to q}(z,z_2) - I_{qg\to q}(0,z_2)\delta(1-z)\Big) \\ &= -\left(\frac{N}{2\pi}\right)\frac{1}{\Gamma(1-\epsilon)}\left(\frac{4\pi\mu^2}{s_{\min}}\right)^{\epsilon}\left(1-\frac{1}{N^2}\right) \\ &\quad\times\frac{1}{\epsilon}\Big[\frac{1}{2}\left(\frac{1+z^2}{[(1-z)^{1+\epsilon}]_+} - \epsilon(1-z)^{1-\epsilon}\right) \\ &\quad + \left(\frac{3}{4} - \epsilon\left(\frac{\pi^2}{6} - \frac{7}{4}\right)\right)\delta(1-z)\Big]. \end{aligned} \tag{3.31}$$

We see that the dependence on the boundaries exactly cancels, making the crossing function independent of the hard process. The other two functions, $X_{g\to q}(z)$ and $X_{q\to g}(z)$, do not receive contributions from the final state crossing,

$$\begin{aligned} X_{g\to q}(z) &= -\left(\frac{N}{2\pi}\right)\frac{1}{\Gamma(1-\epsilon)}\left(\frac{4\pi\mu^2}{s_{\min}}\right)^{\epsilon}\frac{1}{\epsilon}J_{g\to q}(z,0) \\ &= -\left(\frac{N}{2\pi}\right)\frac{1}{\Gamma(1-\epsilon)}\left(\frac{4\pi\mu^2}{s_{\min}}\right)^{\epsilon}\frac{1}{\epsilon}\left(\tfrac{1}{4}\widehat{P}_{q\bar q\to g}(z)(1-z)^{-\epsilon}\right), \end{aligned}$$

$$X_{q\to g}(z) = -\left(\frac{N}{2\pi}\right)\frac{1}{\Gamma(1-\epsilon)}\left(\frac{4\pi\mu^2}{s_{\min}}\right)^{\epsilon}\frac{1}{\epsilon}J_{q\to g}(z,0)$$
$$= -\left(\frac{N}{2\pi}\right)\frac{1}{\Gamma(1-\epsilon)}\left(\frac{4\pi\mu^2}{s_{\min}}\right)^{\epsilon}\frac{1}{\epsilon}\left(\tfrac{1}{4}\widehat{P}_{gq\to q}(z)(1-z)^{-\epsilon}\right). \tag{3.32}$$

Here, we have replaced endpoints that do not contribute with a zero [that is, we have simply dropped contributions of $O(s_{\min})$].

We have now derived the process independent crossing functions. They still contain the mass singularity, which has to be removed by the mass factorization prescription. In fact in the language we have developed here the mass factorization is done very easily as is shown in the next subsection.

3.4. MASS FACTORIZATION

The only physical, and therefore finite, quantity associated with resolved partons is the effective structure function $\mathcal{F}_h^H(x)$ as defined in eq. (2.11). Conventionally, the parton density function is made finite by renormalizing the parton density function at the factorization scale μ_F,

$$f_h^H(x) = f_h^H(x,\mu_F) - \alpha_s\sum_p\int_x^1\frac{dz}{z}f_p^H(x/z,\mu_F)R_{p\to h}(z,\mu_F) + O(\alpha_s^2). \tag{3.33}$$

This is very similar to coupling constant renormalization. The $O(\alpha_s)$ term is subsequently absorbed in the crossing function,

$$\mathcal{F}_h^H(x) = f_h^H(x) + \alpha_s C_h^H(x)$$
$$= f_h^H(x,\mu_F) + \alpha_s C_h^H(x,\mu_F) + O(\alpha_s^2), \tag{3.34}$$

with

$$C_h^H(x,\mu_F) = \sum_p\int_x^1\frac{dz}{z}f_h^H(x/z,\mu_F)\left(X_{p\to h}(z) + R_{p\to h}(z,\mu_F)\right), \tag{3.35}$$

where the mass factorization counterfunction absorbs the divergences in the crossing functions. Note that the effective structure function, $\mathcal{F}_h^H$, is left unchanged by the mass factorization and is in fact independent of the factorization scale. However, for a cross section calculated at fixed order in perturbation theory, we have to expand the effective structure functions explicitly and neglect terms of $O(\alpha_s^2)$ as was done in eq. (2.12). This makes the fixed order cross section factorization scale dependent since we have to neglect the term $\alpha_s^2(\mu_F)C_a^{H_1}(x_1,\mu_F)C_b^{H_2}(x_2,\mu_F)$.

The mass factorization counterfunctions $R_{p\to h}$ at the factorization scale μ_F are given by

$$
\begin{aligned}
R^{\text{scheme}}_{g\to g}(z,\mu_F) &= \left(\frac{N}{2\pi}\right)\left(\frac{4\pi\mu^2}{\mu_F^2}\right)^{\epsilon}\frac{1}{\Gamma(1-\epsilon)}\frac{1}{\epsilon}\\
&\quad\times\left\{\frac{(11N-2n_f)}{6N}\delta(1-z)\right.\\
&\quad\left.+2\left(\frac{z}{(1-z)_+}+\frac{(1-z)}{z}+z(1-z)\right)+\epsilon f^{\text{scheme}}_{g\to g}(z)\right\},\\
R^{\text{scheme}}_{q\to q}(z,\mu_F) &= \left(\frac{N}{2\pi}\right)\left(\frac{4\pi\mu^2}{\mu_F^2}\right)^{\epsilon}\frac{1}{\Gamma(1-\epsilon)}\frac{1}{\epsilon}\left(1-\frac{1}{N^2}\right)\\
&\quad\times\left\{\frac{3}{4}\delta(1-z)+\frac{1}{2}\left(\frac{1+z^2}{(1-z)_+}\right)+\epsilon f^{\text{scheme}}_{q\to q}(z)\right\},\\
R^{\text{scheme}}_{g\to q}(z,\mu_F) &= \left(\frac{N}{2\pi}\right)\left(\frac{4\pi\mu^2}{\mu_F^2}\right)^{\epsilon}\frac{1}{\Gamma(1-\epsilon)}\frac{1}{\epsilon}\left\{\tfrac{1}{4}\widehat{P}^4_{q\bar{q}\to g}(z)+\epsilon f^{\text{scheme}}_{g\to q}(z)\right\},\\
R^{\text{scheme}}_{q\to g}(z,\mu_F) &= \left(\frac{N}{2\pi}\right)\left(\frac{4\pi\mu^2}{\mu_F^2}\right)^{\epsilon}\frac{1}{\Gamma(1-\epsilon)}\frac{1}{\epsilon}\left\{\tfrac{1}{4}\widehat{P}^4_{gq\to q}(z)+\epsilon f^{\text{scheme}}_{q\to g}(z)\right\},
\end{aligned}
\tag{3.36}
$$

where the four dimensional part of the splitting function is given by $\widehat{P}^4_{ab\to c}(z)$ and $\widehat{P}^{\epsilon}_{ab\to c}(z)$ is the $d-4$ part. The function $f^{\text{scheme}}_{p\to h}(z)$ is the scheme dependent mass factorization term chosen such that $f^{\overline{\text{MS}}}_{p\to h}(z)=0$. The strong coupling constant in (3.32) is evaluated at the scale μ, which through coupling constant renormalization is identified with the renormalization scale. Other choices of the scale are possible, however, provided $\alpha_s\log(\mu_R^2/\mu_F^2)\ll 1$, the difference is of $O(\alpha_s^2)$ and can be ignored. Indeed, this condition is necessary in order to prevent the appearance of large logarithms. In practice, μ_R and μ_F will usually be chosen equal, but if they are not, the ratio μ_R/μ_F should be small.

Combining the unrenormalized crossing functions of eqs. (3.31) and (3.32) with the counterfunctions of eq. (3.36) gives us the finite, renormalized crossing functions in the $\overline{\text{MS}}$ scheme,

$$
C_h^{H,\overline{\text{MS}}}(x,\mu_F)=\left(\frac{N}{2\pi}\right)\left[A_h^H(x,\mu_F)\log\left(s_{\min}/\mu_F^2\right)+B_h^{H,\overline{\text{MS}}}(x,\mu_F)\right],
\tag{3.37}
$$

where the arbitrary scale μ has cancelled and

$$
\begin{aligned}
A_h^H(x,\mu_F) &= \sum_p A^H_{p\to h}(x,\mu_F),\\
B_h^{H,\overline{\text{MS}}}(x,\mu_F) &= \sum_p B^{H,\overline{\text{MS}}}_{p\to h}(x,\mu_F).
\end{aligned}
\tag{3.38}
$$

The finite scheme independent functions $A^H_{p\to h}(x,\mu_F)$ are given by

$$
\begin{aligned}
A^H_{g\to g}(x,\mu_F) &= \int_x^1 \frac{dz}{z} f_g^H(x/z,\mu_F)\left\{\frac{(11N-2n_f)}{6N}\delta(1-z)\right.\\
&\quad \left. + 2\left(\frac{z}{(1-z)_+} + \frac{(1-z)}{z} + z(1-z)\right)\right\},\\
A^H_{q\to q}(x,\mu_F) &= \int_x^1 \frac{dz}{z} f_q^H(x/z,\mu_F)\left(1-\frac{1}{N^2}\right)\\
&\quad \times\left\{\tfrac{3}{4}\delta(1-z) + \frac{1}{2}\left(\frac{1+z^2}{(1-z)_+}\right)\right\},\\
A^H_{g\to q}(x,\mu_F) &= \int_x^1 \frac{dz}{z} f_g^H(x/z,\mu_F)\,\tfrac{1}{4}\hat{P}^4_{q\bar{q}\to g}(z),\\
A^H_{q\to g}(x,\mu_F) &= \int_x^1 \frac{dz}{z} f_q^H(x/z,\mu_F)\,\tfrac{1}{4}\hat{P}^4_{gq\to q}(z),
\end{aligned}
\tag{3.39}
$$

and the scheme dependent functions $B^{H,\overline{MS}}_{p\to h}(x)$ by

$$
\begin{aligned}
B^{H,\overline{MS}}_{g\to g}(x,\mu_F) &= \int_x^1 \frac{dz}{z} f_g^H(x/z,\mu_F)\\
&\quad \times\left\{\left(\frac{\pi^2}{3} - \frac{67}{18} + \frac{5n_f}{9N}\right)\delta(1-z) + 2z\left(\frac{\log(1-z)}{(1-z)}\right)_+\right.\\
&\quad \left. + 2\left(\frac{(1-z)}{z} + z(1-z)\right)\log(1-z)\right\},\\
B^{H,\overline{MS}}_{q\to q}(x,\mu_F) &= \int_x^1 \frac{dz}{z} f_q^H(x/z,\mu_F)\left(1-\frac{1}{N^2}\right)\\
&\quad \times\left\{\left(\tfrac{1}{6}\pi^2 - \tfrac{7}{4}\right)\delta(1-z) - \tfrac{1}{2}(1-z)\right.\\
&\quad \left. + \tfrac{1}{2}(1+z^2)\left(\frac{\log(1-z)}{(1-z)}\right)_+\right\},\\
B^{H,\overline{MS}}_{g\to q}(x,\mu_F) &= \frac{1}{4}\int_x^1 \frac{dz}{z} f_g^H(x/z,\mu_F)\left\{\hat{P}^4_{q\bar{q}\to g}(z)\log(1-z) - \hat{P}^c_{q\bar{q}\to g}(z)\right\},\\
B^{H,\overline{MS}}_{q\to g}(x,\mu_F) &= \frac{1}{4}\int_x^1 \frac{dz}{z} f_q^H(x/z,\mu_F)\left\{\hat{P}^4_{gq\to q}(z)\log(1-z) - \hat{P}^c_{gq\to q}(z)\right\}.
\end{aligned}
\tag{3.40}
$$

With these formulae we can calculate the crossing functions for each set of given parton density functions. These crossing functions are independent of the hard process. It is now straightforward to evaluate $A_h(x,\mu_F)$, $B_h(x,\mu_F)$ and $C_h(x,\mu_F)$ numerically for a given set of input parton density functions in a

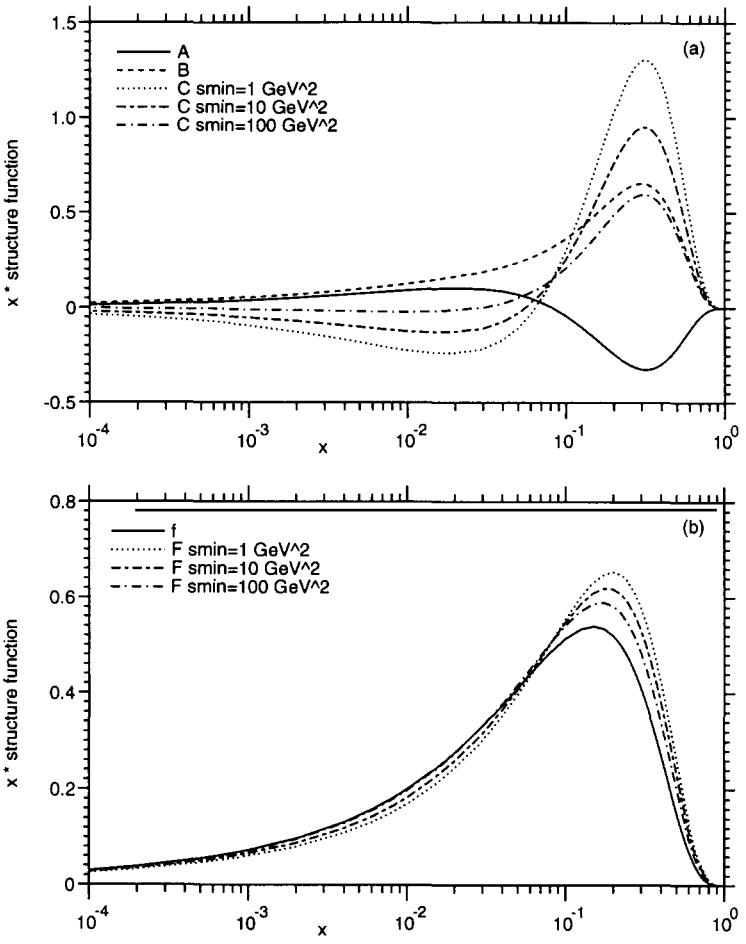

Fig. 1. The valence quark density functions (a) A_u, B_u and C_u and (b) $\mathcal{F}_u$ and f_u as a function of x for $\mu_F = 25$ GeV. C_u and $\mathcal{F}_u$ are shown for $s_{min} = 1$, 10 and 100 GeV^2.

particular scheme. We use the $\overline{MS}$ scheme, and in order to give some idea of the size and relative importance of the crossing functions we use set B1 of ref. [31] as input proton $\overline{MS}$ parton density functions. Furthermore, we focus on the crossing functions associated with valence up quarks and gluons. The distributions for down valence quarks show a similar behavior to the up valence quarks while the sea quarks are related to the gluonic distributions.

First, we show the x dependence of the crossing functions for valence up quarks at a fixed scale $\mu_F = 25$ GeV in fig. 1. In order to illustrate the s_{min} dependence of C_u, three values of s_{min} have been chosen, $s_{min} = 1$, 10 and 100 GeV^2. The first two values are typical of the s_{min} chosen in practical applications (see section 4) and are values where the systematic uncertainty in

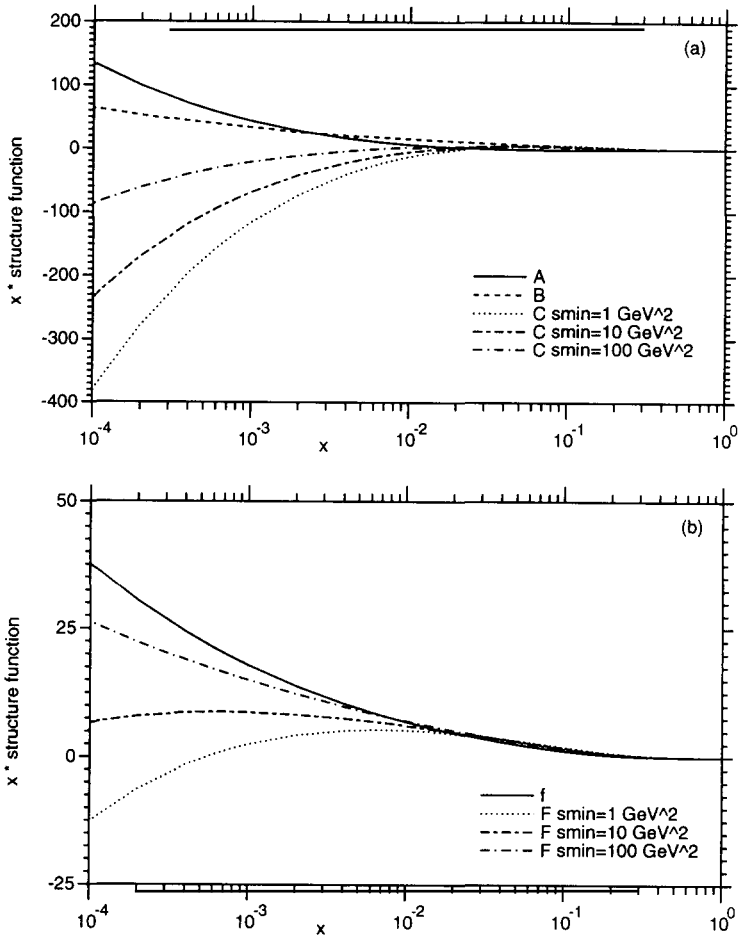

Fig. 2. The gluon density functions (a) A_g, B_g and C_g and (b) $\mathcal{F}_g$ and f_g as a function of x for $\mu_F = 25$ GeV. C_g and $\mathcal{F}_g$ are shown for $s_{min} = 1$, 10 and 100 GeV^2.

evaluating the cross section is of the same order as the uncertainty introduced by approximating the matrix elements at small s_{min}. Although C_u does explicitly depend on this unphysical parameter, this dependence is balanced by a growth of the bremsstrahlung contribution to the next-to-leading cross section. Once this cancellation takes place, s_{min} is replaced by a scale of order of the experimental cuts. For jets with $E_T \geqslant E_{T,min} \sim O(15\ \text{GeV})$ and a jet–jet separation of $\Delta R \sim 0.7$, this scale is of order $E^2_{T,min}\Delta R^2 \sim O(100\ \text{GeV}^2)$. The curves with $s_{min} = 100\ \text{GeV}^2$ are representative of such a scale and give some indication of the contribution to the physical cross section. As shown in fig. 1a, both A_u and C_u are negative for some values of x. Although this seems somewhat strange, A_u and C_u are not directly interpretable as physical distribution; only the com-

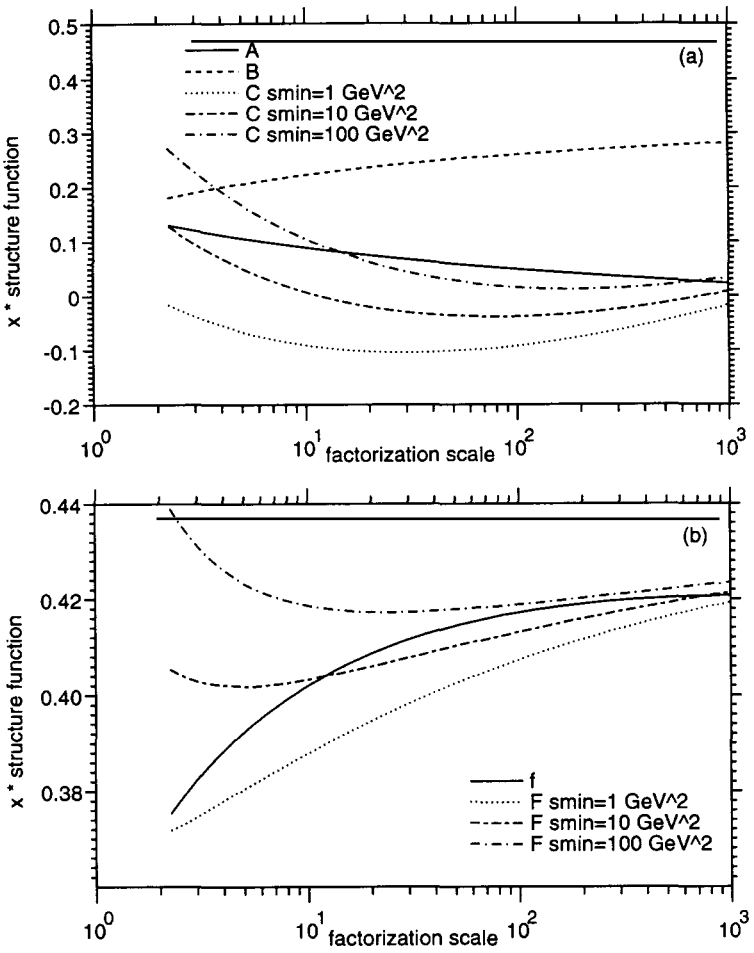

Fig. 3. The valence quark density functions (a) A_u, B_u and C_u and (b) $\mathcal{F}_u$ and f_u as a function of the factorization scale μ_F in GeV for $x = 0.05$. C_u and $\mathcal{F}_u$ are shown for $s_{min} = 1$, 10 and 100 GeV^2.

plete next-to-leading order cross section as defined in eq. (2.12) is expected to be positive (so long as higher-order corrections are not too large). It is worth noting that although A_u and $B_u^{\overline{MS}}$ are roughly similar in size, the contribution of A_u to C_u is enhanced by $\log(s_{min}/\mu_F^2)$ which can be large. Therefore, particularly for small s_{min}, the shape of C_u is dictated by the scheme independent function A_u, while B_u is only important as $s_{min} \to \mu_F^2$. As mentioned earlier, a more physical quantity is the effective structure function $\mathcal{F}_u$ defined in eq. (2.11). This is shown in fig. 1b for the same three values of s_{min} as is the ordinary parton density function f_u. We see that at large x, $\mathcal{F}_u$ is enhanced relative to f_u, while at small x there is a depletion. Furthermore, as $s_{min} \to \mu_F^2$, $\mathcal{F}_u$ approaches f_u. Note

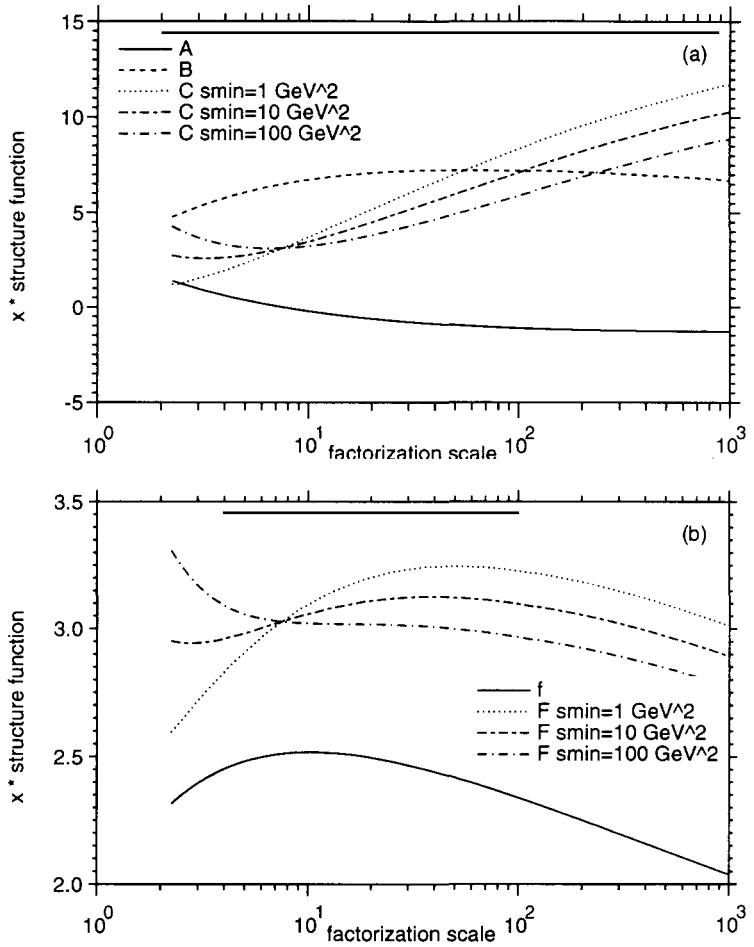

Fig. 4. The gluon density functions (a) A_g, B_g and C_g and (b) $\mathcal{F}_g$ and f_g as a function of the factorization scale μ_F in GeV for $x = 0.05$. C_g and $\mathcal{F}_g$ are shown for $s_{\min} = 1$, 10 and 100 GeV^2.

that for very small factorization scales such that $\mu_F^2 < s_{\min}$, then $\mathcal{F}_u$ is depleted at large x and enhanced at small x.

Figure 2 shows the x distribution for the gluonic crossing functions. These crossing functions receive contributions from both $g \to gg$ and $q \to gq$ splitting functions, and, due to the soft gluon poles that are present, A_g and B_g both grow at small x. As a consequence, C_g is negative in this region. However, for large $s_{\min}$, there is a significant cancellation between A_g and B_g so that C_g is less singular. This is reflected in fig. 2b, where $\mathcal{F}_g$ and f_g are shown for the gluon. At small x there is a dramatic softening of the growth of the gluon density function. This depletion is entirely consistent with the depletion of the up valence distribution discussed above. Similarly, at large x, there is a small enhancement.

It is also instructive to study the scale dependence of the crossing functions. This dependence is present in the input parton density functions and hence A and B and through the $\log(s_{\min}/\mu_F^2)$ factor multiplying A in eq. (3.37). $\mathcal{F}$ contains an additional μ_F dependence from the strong coupling constant evaluated at the factorization scale, which we take to be equal to the renormalization scale. Figure 3 shows the μ_F dependence for the up valence density functions at $x = 0.05$. A_u is a slowly decreasing function, much smaller than B_u while both A_u and B_u are positive for $\mu_F < 1000$ GeV. As a consequence, for $s_{\min} < \mu_F^2$, C_u is relatively small due to a cancellation between the two terms. This is not the case for smaller scales where C_u can be quite large. Figure 3b again shows the ordinary parton density function f_u with the effective structure function $\mathcal{F}_u$. For large μ_F, where C_u is small, f_u and $\mathcal{F}_u$ are very similar in size, while at small scales we can see very large differences.

The scale dependence of the gluonic crossing functions is shown in fig. 4. Unlike the up valence quark case, A_g becomes negative at a scale of $\mu_F = 7$ GeV. As a consequence, A_g and the rather large B_g combine together coherently to form C_g which grows logarithmically at large scales. Furthermore, the effective structure function $\mathcal{F}_g$ is always significantly larger than the ordinary parton density function f_g.

4. Applications

We turn next to the construction of an example of a next-to-leading order cross sections for jet production at hadron colliders. Let us focus on the process

$$V \to q\bar{q} + n\ g, \tag{4.1}$$

for which the lowest order matrix element is given by

$$\mathcal{M}_V(Q_1; 1, \ldots, n; \overline{Q}_2 | P) = \hat{S}_\mu(Q_1; 1, \ldots, n; \overline{Q}_2) V^\mu. \tag{4.2}$$

Here V^μ represents either the vector boson polarization vector, the lepton current which created the vector boson, or the leptonic decay products of the vector boson, while $\hat{S}_\mu$ is the hadron current. Both currents depend on the particle helicities, which we suppress throughout, and the particle momenta, which we denote by P for the vector boson, Q_1, $\overline{Q}_2$ for the quarks and $K_1, \ldots, K_n$ for the gluons. These momenta satisfy the momentum conservation relation

$$P^\mu = Q_1^\mu + \overline{Q}_2^\mu + K_1^\mu + \ldots + K_n^\mu. \tag{4.3}$$

In addition, the hadron current depends on the colors of the gluons $a_1, \ldots, a_n$ and the quarks c_1, c_2.

The hadron current $\hat{S}_\mu$ may be decomposed according to the different allowed

color structures [6–8],

$$\widehat{\mathcal{S}}_\mu(Q_1;1,\ldots,n;\overline{Q}_2) = ieg^n \sum_{P(1,\ldots,n)} (T^{a_1}\ldots T^{a_n})_{c_1\bar{c}_2}\mathcal{S}_\mu(Q_1;1,\ldots,n;\overline{Q}_2), \tag{4.4}$$

where $\mathcal{S}_\mu$ represents the colorless ordered amplitude in which the gluons are emitted in an ordered way from the quark line. Note that the prefactor associated with each $\mathcal{S}_\mu$ is also ordered according to the color of the gluons. These color factors form a complete basis and therefore each $\mathcal{S}_\mu$ is gauge invariant with respect to the gluons. Although the full hadron current $\widehat{\mathcal{S}}_\mu$ is invariant under permutations of the gluons, the ordered amplitude is not. This property is recovered by summing the ordered amplitudes over the $n!$ gluon permutations $P(1,\ldots,n)$.

One advantage of using this color decomposition is that the squared matrix elements summed over helicities and colors have a very systematic structure,

$$|\mathcal{M}_V|^2 = \left|\widehat{\mathcal{S}}_\mu V^\mu\right|^2 = e^2\left(\tfrac{1}{2}g^2N\right)^n\left(\frac{N^2-1}{N}\right)\left[\sum_{P(1,\ldots,n)}\left|\mathcal{S}_\mu V^\mu\right|^2 + \mathrm{O}\left(\frac{1}{N^2}\right)\right], \tag{4.5}$$

where $n \geqslant 1$ counts the number of gluons. On the right hand side, we have expanded in the number of colors. The terms subleading in the number of colors are related to matrix elements with abelian couplings. For example, when $n = 2$,

$$\left|\widehat{\mathcal{S}}_\mu(Q_1;1,2;\overline{Q}_2)V^\mu\right|^2 = e^2\left(\tfrac{1}{2}g^2N\right)^2\left(\frac{N^2-1}{N}\right) \times\left[\sum_{P(1,2)}\left|\mathcal{S}_\mu(Q_1;1,2;\overline{Q}_2)V^\mu\right|^2 - \frac{1}{N^2}\left|\mathcal{S}_\mu(Q_1;\tilde{1},\tilde{2};\overline{Q}_2)V^\mu\right|^2\right], \tag{4.6}$$

where

$$\mathcal{S}_\mu(Q_1;\tilde{1},\tilde{2};\overline{Q}_2) = \mathcal{S}_\mu(Q_1;1,2;\overline{Q}_2) + \mathcal{S}_\mu(Q_1;2,1;\overline{Q}_2), \tag{4.7}$$

and the contribution from the triple gluon vertex drops out. The Feynman graphs contributing to $\mathcal{S}_\mu(Q_1;\tilde{1},\tilde{2};\overline{Q}_2)$ are therefore those for $V \to q\bar{q} + 2\gamma$ or $V \to q\bar{q} + g + \gamma$.

The ordered amplitudes also have special properties in the soft gluon or collinear parton limits which allow us to isolate the singular regions using the parton resolution parameter $s_{\min}$ [18,14]. These divergences are proportional to the lowest order squared ordered amplitudes as are the virtual divergences. Therefore we can combine them directly and, due to the Kinoshita–Lee–Nauenberg [28,29] theorems, obtain a finite result after the usual coupling constant renor-

malization. The finite next-to-leading order matrix elements can be written

$$\left|\widehat{\mathcal{S}}_\mu V^\mu\right|_{\mathrm{F}}^2 = e^2\left(\tfrac{1}{2}g^2N\right)^n\left(\frac{N^2-1}{N}\right) \times \sum_{P(1,\ldots,n)}\Bigg[\mathcal{K}(Q_1;1,\ldots,n;\overline{Q}_2)\left|\mathcal{S}_\mu(Q_1;1,\ldots,n;\overline{Q}_2)V^\mu\right|^2 + \mathcal{F}(Q_1;1,\ldots,n;\overline{Q}_2) + \mathrm{O}\left(1/N^2\right)\Bigg], \tag{4.8}$$

where $\mathcal{F}(Q_1;1,\ldots,n;\overline{Q}_2)$ is the finite contribution from the virtual graphs. The dynamical ordered $\mathcal{K}$ factor is given by

$$\mathcal{K}(Q_1;1,\ldots,n;\overline{Q}_2) = \left(\frac{\alpha_{\mathrm{s}}(\mu_{\mathrm{R}}^2)N}{2\pi}\right) \times \Bigg[\sum_{ij}\left\{-\log^2\left(|s_{ij}|/s_{\min}\right) + \tfrac{1}{2}\pi^2\left(\Theta(s_{ij}) - \tfrac{2}{3}\right)\right\} + \tfrac{3}{4}\log\left(|s_{Q_1 1}|/s_{\min}\right) + \tfrac{3}{4}\log\left(|s_{n\overline{Q}_2}|/s_{\min}\right) + \frac{67n-9}{18} - \frac{5nn_{\mathrm{f}}}{9N}\Bigg] + \alpha_{\mathrm{s}}(\mu_{\mathrm{R}}^2)b_0 n\log\left(\mu_{\mathrm{R}}^2/s_{\min}\right) + \mathrm{O}(\epsilon) + \mathrm{O}(s_{\min}), \tag{4.9}$$

where the sum runs over all $(n+1)$ color-connected pairs, that is, $ij = Q_1 1, 12, \ldots, n\overline{Q}_2$, and where b_0 is the one-loop coefficient of the QCD beta function. Note that $\mathcal{K}(Q_1;1,\ldots,n;\overline{Q}_2)$ depends explicitly on the parton resolution parameter $s_{\min}$. The renormalization scale μ_{R} is the scale at which the $\overline{\mathrm{MS}}$ counter term is subtracted. For vector boson decay all $s_{ij} > 0$ so that $\Theta(s_{ij}) = 1$. However, when we cross partons into the initial state this will no longer be true and it is necessary to maintain the explicit analytic continuations of the $\log^2$ terms. Up to this point, we have continued both matrix elements and phase space into $d = 4 - 2\epsilon$ using dimensional regularization. In eq. (4.9), we now see that all singularities have cancelled explicitly and we may therefore take the four-dimensional limit. This means that the squared ordered amplitudes, $|\mathcal{S}_\mu V^\mu|^2$, may be evaluated in four dimensions and not in d dimensions, thus simplifying the calculation dramatically. Similarly, it is not necessary to extend the jet algorithm to d dimensions as in the work of Ellis, Kunszt, and Soper [21].

Keeping all orders in the number of colors presents no problems. For example, the effective matrix elements for $V \to q\overline{q} + 2g$ at next-to-leading order are given

by

$$\left|\widehat{\mathcal{S}}_\mu V^\mu\right|^2_{\mathrm{F}} = e^2\left(\tfrac{1}{2}g^2N\right)^2\left(\frac{N^2-1}{N}\right)$$
$$\times\left[\sum_{P(1,2)}\left(\mathcal{K}(Q_1;1,2;\overline{Q}_2)-\frac{1}{N^2}\mathcal{K}(Q_1;\overline{Q}_2)\right)\left|\mathcal{S}_\mu(Q_1;1,2;\overline{Q}_2)V^\mu\right|^2\right.$$
$$-\frac{1}{N^2}\left(\mathcal{K}(Q_1;1;\overline{Q}_2)+\mathcal{K}(Q_1;2;\overline{Q}_2)-\left(1+\frac{1}{N^2}\right)\mathcal{K}(Q_1;\overline{Q}_2)\right)$$
$$\left.\times\left|\mathcal{S}_\mu(Q_1;\tilde{1},\tilde{2};\overline{Q}_2)V^\mu\right|^2\right]+\mathcal{F}(Q_1;1,2;\overline{Q}_2), \tag{4.10}$$

where $\mathcal{K}(Q_1;\overline{Q}_2)$, $\mathcal{K}(Q_1;1;\overline{Q}_2)$ and $\mathcal{K}(Q_1;1,2;\overline{Q}_2)$ are given by eq. (4.9) with $n = 0, 1$ and 2, respectively.

4.1. $H_1H_2 \to V + 0$ JETS

As a first application of 2.12 and the next-to-leading order crossing approach, let us consider the production of a vector boson in hadron-hadron collisions followed by the decay of the vector boson in the absence of jets. The relevant parton-level processes are

$$q\bar{q} \to V, \tag{4.11}$$

along with the bremsstrahlung processes

$$q\bar{q} \to V + g,\ qg \to V + q,\ g\bar{q} \to V + \bar{q}, \tag{4.12}$$

for which the generic cross section is given by

$$\mathrm{d}\sigma_{ab}(x_1,x_2) = \frac{\Phi_{ab}}{2s_{ab}}|\mathcal{M}_{ab}|^2\ \mathrm{d}P(ab \to V + 0,\ 1\,\text{partons}). \tag{4.13}$$

The spin and color averaging factors, Φ_{ab}, are given by

$$\Phi_{q\bar{q}} = \frac{1}{4N^2},\ \Phi_{qg} = \Phi_{g\bar{q}} = \frac{1}{4N(N^2-1)},\ \Phi_{gg} = \frac{1}{4(N^2-1)^2}. \tag{4.14}$$

The lowest order matrix elements for these processes are related to those for eq. (4.1) with $n = 0$ and 1 through the usual crossing relations. In other words, the momenta and helicity of crossed particles are reversed. For example,

$$\left|\mathcal{M}_{q\bar{q}}(Q_1;1,\ldots,n;\overline{Q}_2|P)\right|^2 = \left|\mathcal{M}_V(-Q_1;1,\ldots,n;-\overline{Q}_2|-P)\right|^2, \tag{4.15}$$

$$\left|\mathcal{M}_{qg}(Q_1;1,\ldots,n;\overline{Q}_2|P)\right|^2 = -\left|\mathcal{M}_V(Q_1;-1,\ldots,n;-\overline{Q}_2|-P)\right|^2. \tag{4.16}$$

An explicit form for these matrix elements and hence $|\mathcal{S}_\mu(Q_1;\overline{Q}_2)V^\mu|^2$ and $|\mathcal{S}_\mu(Q_1;1;\overline{Q}_2)V^\mu|^2$ using spinor language is given in appendix A of ref. [14]. Full details of how crossing affects the spinors are given in appendix E of ref. [32].

At next-to-leading order, the finite effective matrix elements for eq. (4.1) with $n = 0$ are given by

$$\left|\mathcal{M}_V(Q_1;\overline{Q}_2|P)\right|_{\mathrm{F}}^2 = e^2 N\left(1-\frac{1}{N^2}\right) \times\left[\mathcal{K}(Q_1;\overline{Q}_2)\left|\mathcal{S}_\mu(Q_1;\overline{Q}_2)V^\mu\right|^2+\mathcal{F}(Q_1;\overline{Q}_2)\right], \quad (4.17)$$

where, because of our choice for the assignment of the finite pieces between $\mathcal{K}$ and $\mathcal{F}$,

$$\mathcal{F}(Q_1;\overline{Q}_2) = 0. \quad (4.18)$$

The dynamical $\mathcal{K}$ factor is given by eq. (4.9) with $n = 0$. Because of eq. (2.12), we may cross this in exactly the same manner as the tree level matrix elements of eq. (4.15). The only subtlety is in the analytic continuation of the $\log^2$ terms in $\mathcal{K}$ which we have written out explicitly in eq. (4.9).

It is now straightforward to construct a Monte Carlo program to evaluate the fully differential cross section numerically. In particular, the vector boson decays are easily included, which allows experimental cuts to be placed directly on the observed leptons. It is important to note that the phase space is restricted to regions where all partons are resolved. In other words, any pair of partons must have an invariant mass larger than the parton resolution parameter, $|s_{ij}| > s_{\min}$. What this means in practical terms is that the bremsstrahlung contribution to the cross section grows as $\log^2(s_{\min})$. This is balanced by the explicit $-\log^2(s_{\min})$ in $\mathcal{K}$ such that the total cross section should be independent of the unphysical $s_{\min}$ provided (a) that $s_{\min}$ is small enough that the soft and collinear approximations are valid and (b) that $s_{\min}$ is not so small that the numerical cancellation between the two contributions becomes unstable. Figure 5 shows that the $O(\alpha_s)$ W + 0 jet or $\ell^\pm + E_{\mathrm{T}}^{\mathrm{missing}} + 0$ jet cross section is essentially independent of $s_{\min}$ over a wide range of $s_{\min}$. In general, one wants to choose the largest $s_{\min}$ possible, to minimize the running time of the program. In this case, a reasonable value to choose is $s_{\min} = 10\ \mathrm{GeV}^2$. (One must be careful to note that for certain distributions, in particular infrared-sensitive ones, a smaller $s_{\min}$ might be required for some values of the relevant kinematic variables.)

One quantity of interest is the dependence of the W + 0 jet cross section on the choice of experimental cuts. In principle, including higher orders mimics more accurately the correct dependence. At leading order, with "standard" CDF cuts,

$$\sigma(\mathrm{W} + 0\ \mathrm{jets}) = 0.78^{+0.01}_{-0.03}\ \mathrm{nb}. \quad (4.19)$$

This does not depend on the jet defining cut, $E_{\mathrm{T,min}}^{\mathrm{jet}}$, since at leading order there is no parton in the final state. At next-to-leading order, this is no longer true and in fig. 6 we show the next-to-leading order $W + 0$ jet cross section as a function of $E_{\mathrm{T,min}}^{\mathrm{jet}}$ for the same range of scales. As $E_{\mathrm{T,min}}^{\mathrm{jet}}$ becomes large, this cross-section approaches the inclusive W cross section.

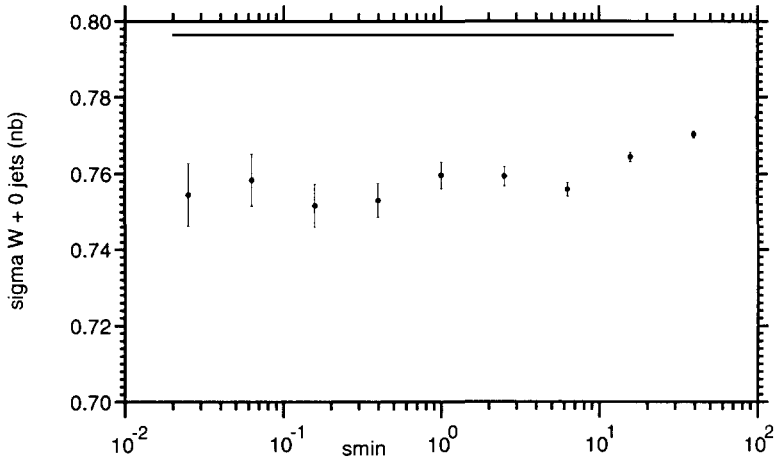

Fig. 5. The $s_{\min}$ dependence of the W + 0 jet cross section for "standard" CDF cuts; $E_T^{jet} \geqslant 15$ GeV, $E_T^{\ell} \geqslant 20$ GeV, $E_u^{missing} > 20$ GeV, $|\eta^{jet}| \leqslant 2$, $|\eta^{\ell}| \leqslant 1$ and a jet cone size $\Delta R = (\Delta\phi^2 + \Delta\eta^2)^{1/2} \leqslant 0.7$. The structure functions are set B1 of ref. [31] while the factorization and renormalization scales are $\mu_F = \mu_R = M_W$. For input parameters we choose $M_u = 80$ GeV, $\Gamma_u = 2$ GeV, $\sin^2\theta_u = 0.23$ and $\alpha_s(M_u) = 0.1108$.

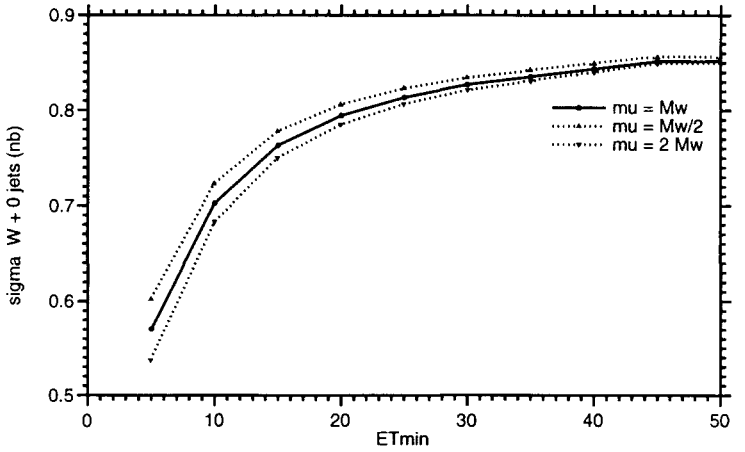

Fig. 6. The NLO W + 0 jet cross section as a function of the jet defining cut $E_{T,min}^{jet}$ for $\mu_F = \mu_R = 2M_u$, M_u and $M_u/2$.

4.2. $H_1H_2 \to V$ + 1 JET

We now turn to vector boson production in association with a single jet. As before, the structure of the next-to-leading cross section is described by eq. (2.12); however, the contributing parton level processes include both those of

eq. (4.12) as well as

$$q\bar{q} \to V + q\bar{q},\ q\bar{q} \to V + gg,\ qg \to V + qg,\ g\bar{q} \to V + g\bar{q},\ gg \to V + q\bar{q}. \tag{4.20}$$

As before, the lowest order matrix elements for eq. (4.20) are obtained by crossing the matrix elements given in appendix A of ref. [14].

The finite next-to-leading order matrix elements are given by

$$\begin{aligned}\left|\mathcal{M}_V(Q_1;1;\overline{Q}_2|P)\right|^2_{\mathrm{F}} &= e^2\left(\tfrac{1}{2}g^2N\right)\left(\frac{N^2-1}{N}\right)\\ &\times\left[\left(\mathcal{K}(Q_1;1;\overline{Q}_2)-\frac{1}{N^2}\mathcal{K}(Q_1;\overline{Q}_2)\right)\left|\mathcal{S}_\mu(Q_1;1;\overline{Q}_2)V^\mu\right|^2\right.\\ &\left.+\mathcal{F}(Q_1;1;\overline{Q}_2)\right],\end{aligned} \tag{4.21}$$

where $\mathcal{K}(Q_1;1;\overline{Q}_2)$ is given by eq. (4.9) with $n = 1$. The finite one loop contributions are given by eqs. (A.42)–(A.46) of ref. [14]. Once again, it is trivial to cross both $\mathcal{K}$ and $|\mathcal{S}_\mu(Q_1;1;\overline{Q}_2)V^\mu|^2$. However, some care must be taken in crossing $\mathcal{F}$ since, although crossing the helicity structure in eq. (A.43) is straightforward, the coefficients α_i, β_i and δ_i in eq. (A.44) are expressed in terms of the function $R(x,y)$ (eq. A.45), which has been written assuming that $0 \leqslant x,y \leqslant 1$. For crossed processes this is no longer true. For example, when

$$x < 0,\ y < 0, \tag{4.22}$$

in which case

$$\begin{aligned}R(x,y) &= -\tfrac{1}{2}\log^2(1-x) - \tfrac{1}{2}\log^2(1-y) + \tfrac{1}{2}\pi^2\\ &\quad -\mathrm{Li}_2\left(\frac{1}{1-x}\right) - \mathrm{Li}_2\left(\frac{1}{1-y}\right).\end{aligned} \tag{4.23}$$

Alternatively, if

$$x < 0,\ y > 1, \tag{4.24}$$

then

$$\begin{aligned}R(x,y) &= -\tfrac{1}{2}\log^2(1-x) + \tfrac{1}{2}\log^2(y) + \log\left(\frac{-x}{y-1}\right)\log(y) + \tfrac{1}{2}\pi^2\\ &\quad -\mathrm{Li}_2\left(\frac{1}{1-x}\right) + \mathrm{Li}_2\left(\frac{1}{y}\right).\end{aligned} \tag{4.25}$$

We have checked that crossed finite virtual contributions agree with the results of Gonsalves et al. [20] when the vector boson decay current is replaced by its polarization vector.

With these crossed matrix elements, we can construct a Monte Carlo program to numerically evaluate the fully differential vector boson plus one jet cross section at next-to-leading order. As before, the vector boson decays are easily

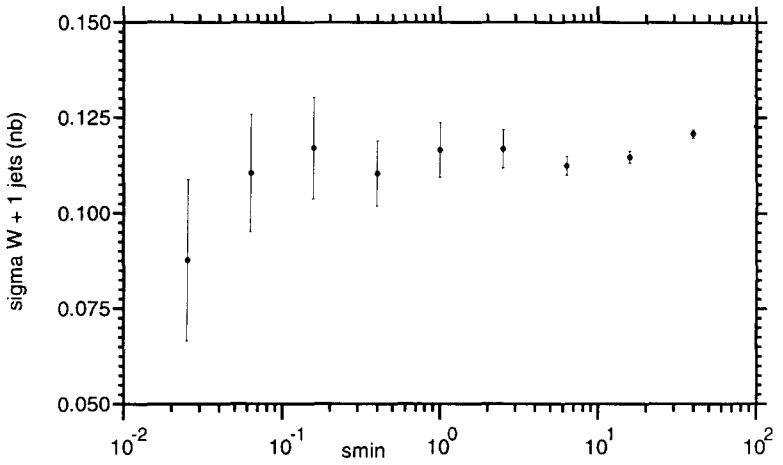

Fig. 7. The $s_{\min}$ dependence of the W + 1 jet cross section for "standard" CDF cuts. The structure functions are set B1 of ref. [31] while the factorization and renormalization scales are $\mu_F = \mu_R = M_u$.

included, which allows experimental cuts to be placed directly on the observed leptons. To demonstrate that the W + 1 jet cross section is essentially independent of the unphysical parameter $s_{\min}$, fig. 7 shows the $O(\alpha_s^2)$ W + 1 jet cross section as a function of $s_{\min}$. For $s_{\min}$ in the range 1–10 GeV^2, the cross section is not dominated by systematic errors and does not depend on $s_{\min}$. We therefore set $s_{\min} = 10$ GeV^2 as in the W + 0 jet case.

An important issue in W + jets events is the significance of corrections to leading order results. For most quantities, radiative effects should be small so that we can rely on leading order to describe the basic features of the data even though the overall normalization of the cross section is uncertain. One of the most fundamental distributions is the jet transverse momentum distribution which is shown in fig. 8.

For the leading order results we choose two renormalization scales, $\mu_R = M_W/2$ and the total invariant mass of the event, $\mu_R = \hat{s}/2$. The first scale is the smallest scale available and generates the hardest transverse momentum distribution while the second scale is the hardest scale available and leads to the softest transverse momentum spectrum. The band defined by these two scales represents the range of leading order predictions. The factor 1/2 is present in the choice of scale so that the corresponding total cross sections at leading order (0.117 nb and 0.106 nb) are close to, and bracket, the next-to-leading order result of 0.113 nb, which is essentially independent of the renormalization scale (here taken to be M_W). As can be seen in fig. 8, the next-to-leading order distribution is somewhat softer than the leading order results. In fact it is even softer than leading order with the largest scale. This implies that the standard jet algorithm

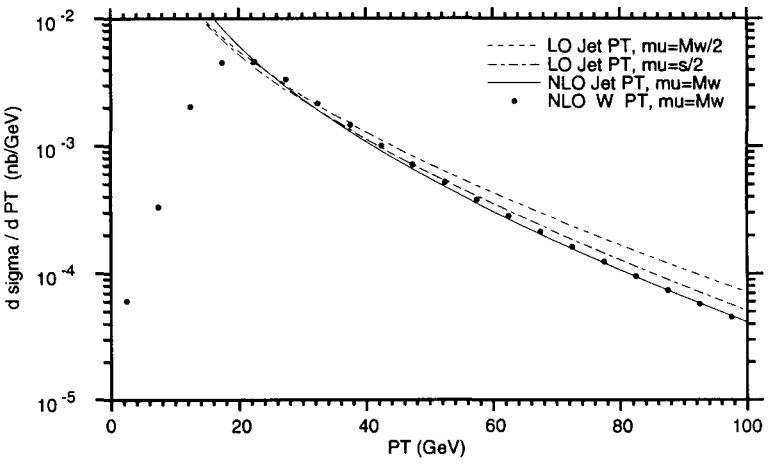

Fig. 8. The $O(\alpha_s)$ and $O(\alpha_s^2)$ jet and W boson transverse momentum distribution for "standard" CDF cuts.

does not take into account an important effect, thereby leading to large radiative effects for high transverse momentum jets.

From a physical point of view, it is clear why the spectrum softens more dramatically than can be expected from leading order with the standard jet algorithm. For high transverse energy jets, the accompanying soft radiation increases with the energy of the jet. Therefore, with a fixed transverse momentum cut (in this case $E_{T,\min}^{jet} = 15$ GeV), it is easier for the soft radiation in the event to fluctuate so that it passes the minimum transverse momentum threshold and subsequently be counted as an extra jet. Since we are looking at the exclusive jet cross section this event will be removed from the W + 1 jet cross section and added to the W + 2 jet cross section. This effect gets more severe when the jet transverse energy gets larger leading to a depletion of the W + 1 jet cross section and a softening of the transverse momentum distribution. At leading order this effect is not modelled at all because the leading order prediction associates all the energy with the jet and allows no soft radiation outside the jet cone. In contrast, at next-to-leading order the hadronic energy around the jet cone is modelled, allowing the generation of softer jets within the tail of high transverse energy jets.

From a more mathematical point of view, it is also clear what happens in the exclusive jet cross section with high transverse momentum jets. From eq. (4.9), we can see that the high transverse momentum jets generate correction terms of order $-\alpha_s \log(E_T^{jet}/E_{T,\min}^{jet})$, which become large if the E_T^{jet} is much larger than the minimal transverse energy. This is undesirable since it implies large radiative effects which are due entirely to the jet algorithm itself. In principle, the jet algorithm should minimize these effects in order to be able to compare theory

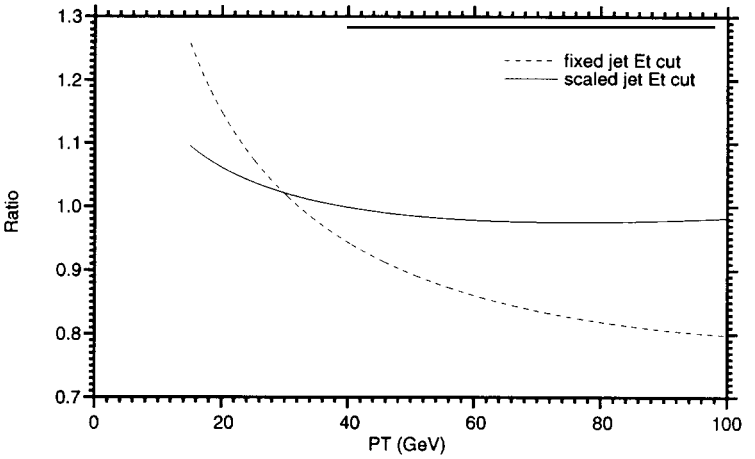

Fig. 9. The ratio of next-to-leading order to leading order jet transverse momentum distributions for a fixed $E_{\mathrm{T,min}}^{\mathrm{jet}} = 15$ GeV cut and for a scaled $E_{\mathrm{T,min}}^{\mathrm{jet}} = \max(15\ \mathrm{GeV}, 0.1 \times \sqrt{\hat{s}})$ cut as a function of the jet transverse momentum.

with experiment.

This requires a slight modification in the jet algorithm. By scaling the minimal transverse momentum cut with the hardness of the event (e.g. summed scalar energies or total invariant mass), we allow the hard jets to radiate accompanying soft energy without generating additional small jets. That is, we allow the jet to "vent" its energy without producing a large number of soft jets. Events which formerly contained W + 2 jets where one of the jets is relatively soft are now counted as W + 1 jet events, thus increasing the W + 1 jet cross section at high transverse momentum. For example, by demanding $E_{\mathrm{T,min}}^{\mathrm{jet}} = \lambda\sqrt{\hat{s}}$, the correction term is $-\alpha_s \log(\lambda)$ where we can now choose the constant λ and thus control the size of the corrections.

To demonstrate this effect we show in fig. 9 the factor with which we need to multiply the leading order distribution (with $\mu_R = \hat{s}/2$) to obtain the next-to-leading order result. For fixed $E_{\mathrm{T,min}}^{\mathrm{jet}}$, we see a sizeable correction that depends strongly on the jet transverse energy. However, if we take a scaling $E_{\mathrm{T,min}}^{\mathrm{jet}} = \max(15\ \mathrm{GeV}, 0.1\ \sqrt{\hat{s}})$, we get a result very close to leading order with only a small enhancement for soft transverse energy jets. For the high transverse energy jets the next-to-leading order prediction is well described by the leading order result.

5. Conclusions

The main theme in this paper is the extension of the general method of ref. [14], for dealing with final state collinear and infrared divergences, to in-

clude partons in the initial state. For final state partons, the soft and collinear divergences from the bremsstrahlung process are isolated using a parton resolution parameter $s_{\min}$. These divergences are proportional to lowest order matrix elements and can be combined directly with the divergences from the virtual graphs to give a finite cross section, eq. (2.4), which depends on a dynamical $\mathcal{K}$ factor multiplying the lowest order term, along with a finite one loop contribution $\mathcal{F}$. In order to extend this to incorporate initial state partons, we have extended the tree level concept of crossing to next-to-leading order processes. This is achieved (a) through the analytic continuation of the dynamical factor $\mathcal{K}$ (eq. 4.9) and the finite one loop contribution $\mathcal{F}$ (see section 4) into the physical region and (b) through the introduction of universal crossing functions, eq. (2.13), which are essentially convolutions of the structure functions with the Altarelli–Parisi splitting functions. Together, $\mathcal{K}$, $\mathcal{F}$ and $C(x)$ form a set of finite building blocks with which one can calculate next-to-leading order cross sections. This is summarized in eq. (2.12); because the ordered factorization of the soft poles and the factorization of the collinear poles is independent of the hard process, this equation represents the general cross section for any hadronic process.

As an explicit example of this method, in section 4, we have taken the next-to-leading order matrix elements relevant for $e^-e^+ \to 2, 3$ and 4 partons [14] and crossed two of the partons into the initial state to obtain the cross section for

$$p\bar{p} \to W^{\pm}Z + 0,\ 1 \text{ jets} \to \ell\bar{\ell} + 0,\ 1 \text{ jets}, \tag{5.1}$$

at next-to-leading order. The phase space is evaluated numerically with the constraint that all $|s_{ij}| > s_{\min}$ and all final state lepton correlations are retained. This makes it possible to implement jet algorithms, detector acceptance effects, and other constraints numerically, yielding a very flexible Monte Carlo program as we discussed in section 4. One should verify that the cross section is independent of the unphysical parameter $s_{\min}$. For our Monte Carlo simulations this is indeed the case, see figs. 5 and 7.

It is important to note that throughout this paper we have discussed cross sections that are exclusive in the number of jets. As a result, we are interested in calculating the W + 0 jet cross section, rather than the inclusive W cross section, which can only be identified with the W + 0 jet cross section as the mimimal transverse energy cut of the jet becomes very large. Similarly, we study the W + 1 jet cross section rather than the transverse momentum distribution of the W boson, which is not directly measurable. As shown in fig. 8, this is not the same as the jet transverse momentum distribution at next-to-leading order. At large E_T^{jet}, the next-to-leading order jet p_u distribution is significantly softened. This is because the existing jet algorithm generates an artificially high jet multiplicity in events containing a very hard jet by restricting the hadronic radiation around the

primary jet in the exclusive jet cross section. By modifying the jet algorithm as described in section 4, these large radiative effects can be removed. A detailed study of the implications of next-to-leading order corrections to vector boson production in association with 0, 1 jets at Fermilab energies is currently in progress [33,34].

The method we have presented here considerably simplifies the structure of next-to-leading order QCD corrections to hadronic processes. It also makes comparison with experiment more direct through the use of Monte Carlo simulations. Once technical problems associated with five point loop diagrams are solved, it should be possible to use these methods to compute processes such as $e^-e^+ \to 4$ jets, its crossing $p\bar{p} \to W^{\pm}Z + 2$ jets and $p\bar{p} \to 3$ jets at next-to-leading order. These multijet cross sections are important for experiments at LEP and Fermilab because event rates are high and can be studied in great detail.

W.T.G is happy to acknowledge financial support from the Texas National Research Laboratory Commission. E.W.N.G would like to thank the Fermilab Theory group for their kind hospitality. We are grateful to Eric Laenen and Keith Ellis for stimulating discussions and for providing a FORTRAN routine for the evaluation of the strong coupling constant. We also thank the Fermilab lattice group for providing us with computer time on the Fermilab ACPMAPS parallel machine.

References

[1] D. Amati and G. Veneziano, Phys. Lett. B83 (1979) 87;
G. Marchesini, L. Trentadue and G. Veneziano, Nucl. Phys. B181 (1981) 335;
Y.I. Azimov, Y.L. Dokshitzer, V.A. Khoze and S.I. Troyan, Z. Phys. C27 (1985) 65

[2] H. Baer, V. Barger and R.J.N. Phillips, Phys. Rev. D39 (1989) 3310;
W.T. Giele and W.J. Stirling, Nucl. Phys. B343 (1990) 14;
F.A. Berends, J.B. Tausk and W.T. Giele, Phys. Rev. D47 (1993) 2747

[3] B.L. Combridge, J. Kripfganz and J. Ranft, Phys. Lett. B70 (1977) 234;
R. Cutler and D. Sivers, Phys. Rev. D17 (1978) 196;
T. Gottschalk and D. Sivers, Phys. Rev. D21 (1980) 102;
Z. Kunszt and E. Pietarinen, Nucl. Phys. B164 (1980) 45;
F.A. Berends, R. Kleiss, P. de Causmaecker, R. Gastmans and T.T. Wu, Phys. Lett. B103 (1981) 124;
J.F. Gunion and Z. Kunszt, Phys. Lett. B159 (1985) 167; B176 (1986) 163;
Z. Kunszt, Nucl. Phys. B271 (1986) 333;
J.F. Gunion and J. Kalinowski, Phys. Rev. D34 (1986) 2119;
S.J. Parke and T.R. Taylor, Nucl. Phys. B269 (1986) 410; Phys. Rev. D35 (1987) 313;
F.A. Berends and W.T. Giele, Nucl. Phys. B294 (1987) 700;
M. Mangano, S.J. Parke and Z. Xu, Nucl. Phys. B298 (1988) 653; B299 (1988) 673;
F.A. Berends, W.T. Giele and H. Kuijf, Phys. Lett. B232 (1989) 266; Nucl. Phys. B333 (1990) 120;
F.A. Berends and H. Kuijf, Nucl. Phys. B353 (1991) 59

[4] R. Kleiss and W.J. Stirling, Nucl. Phys. B262 (1985) 235;
K. Hagiwara and D. Zeppenfeld, Nucl. Phys. B313 (1989) 560;

F.A. Berends, W.T. Giele and H. Kuijf, Nucl. Phys. B321 (1989) 39;
F.A. Berends, W.T. Giele, H. Kuijf and B. Tausk, Nucl. Phys. B357 (1991) 32
[5] P. de Causmaecker, R. Gastmans, W. Troost and T.T. Wu, Phys. Lett. B105 (1981) 215;
R. Kleiss, Nucl. Phys. B241 (1984) 61;
F.A. Berends, P.H. Daverveldt and R. Kleiss, Nucl. Phys. B253 (1985) 441;
J.F. Gunion and Z. Kunszt, Phys. Lett. B161 (1985) 333;
Z. Xu, D.H. Zhang and L. Chang, Nucl. Phys. B291 (1987) 392
[6] F.A. Berends and W.T. Giele, Nucl. Phys. B294 (1987) 700
[7] M. Mangano, S.J. Parke and Z. Xu, Nucl. Phys. B299 (1988) 673
[8] D. Zeppenfeld, Int. J. Mod. Phys. A 3 (1988) 2175
[9] F.A. Berends and W.T. Giele, Nucl. Phys. B306 (1988) 759
[10] J.G.M. Kuijf, Ph.D. thesis, Leiden (1991)
[11] See, for example, CDF Collaboration, F. Abe et al., Phys. Rev. D45 (1992) 1448
[12] H. Baer, J. Ohnemus and J.F. Owens, Phys. Rev. D40 (1989) 2844; Phys. Lett. B234 (1990) 127; Phys. Rev. D42 (1990) 61
[13] F. Aversa, P. Chiappetta, M. Greco and J.Ph. Guillet, Nucl. Phys. B327 (1989) 105; Phys. Rev. Lett. 65 (1990) 401; Z. Phys. C46 (1990) 253; C49 (1991) 459
[14] W.T. Giele and E.W.N. Glover, Phys. Rev. D46 (1992) 1980
[15] R.K. Ellis, D.A. Ross and A.E. Terrano, Nucl. Phys. B178 (1981) 421
[16] Z. Kunszt and D.E. Soper, Phys. Rev. D46 (1992) 196
[17] M. Mangano, P. Nason and G. Ridolfi, Nucl. Phys. B373 (1992) 295
[18] M. Mangano and S.J. Parke, Proc. Int. Europhysics Conf. on High Energy Physics, Uppsala (1987);
F.A. Berends and W.T. Giele, Nucl. Phys. B313 (1989) 595
[19] P. Arnold and M.H. Reno, Nucl. Phys. B319 (1989) 37
[20] R.J. Gonsalves, J. Pawlowski and C.F. Wai, Phys. Rev. D40 (1989) 2245
[21] S.D. Ellis, Z. Kunszt and D.E. Soper, Phys. Rev. D40 (1989) 2188; Phys. Rev. Lett. 64 (1990) 2121
[22] H. Baer and M.H. Reno, Florida State report FSU-HEP-901030 (1990)
[23] S.D. Ellis, Z. Kunszt and D.E. Soper, Phys. Rev. Lett. 69 (1992) 1496
[24] W.A. Bardeen, A.J. Buras, D.W. Duke and T. Muta, Phys. Rev. D18 (1978) 3998
[25] D.R. Yennie, S.C. Frautschi and H. Suura, Ann. Phys. 13 (1961) 379
[26] G. 't Hooft and M. Veltman, Nucl. Phys. B44 (1972) 189
[27] C.G. Bollini and J.J. Giambiagi, Phys. Lett. B40 (1972) 566;
J.F. Ashmore, Nuovo Cim. Lett. 4 (1972) 289
[28] T. Kinoshita, J. Math. Phys. 3 (1962) 650;
T.D. Lee and M. Nauenberg, Phys. Rev. 133 (1964) 1549.
[29] G. Sterman, Phys. Rev. D17 (1978) 2773, 2789
[30] G. Altarelli and G. Parisi, Nucl. Phys. B126 (1977) 298
[31] J.G. Morfin and W.K. Tung, Z. Phys. C52 (1991) 13
[32] F.A. Berends, W.T. Giele and H. Kuijf, Nucl. Phys. B321 (1989) 39
[33] W.T. Giele, E.W.N. Glover and D.A. Kosower, Fermilab report FERMILAB-Conf-92/213-T (1992)
[34] W.T. Giele, E.W.N. Glover and D.A. Kosower, Implications of radiative corrections to lepton production at the Fermilab collider, Fermilab report FERMILAB-Pub-92/229-T (1992)